Remote Sensing of Environment 271 (2022) 112887

Contents lists available at ScienceDirect

Remote Sensing of Environment

journal homepage: www.elsevier.com/locate/rse

Mapping invasive alien species in grassland ecosystems using airborne imaging spectroscopy and remotely observable vegetation functional traits

Hamed Gholizadeh [a,*], Michael S. Friedman [b,1], Nicholas A. McMillan [c,1], William M. Hammond [d,e,1], Kianoosh Hassani [a], Aisha V. Sams [c], Makyla D. Charles [f], DeAndre R. Garrett [e], Omkar Joshi [c], Robert G. Hamilton [g], Samuel D. Fuhlendorf [c], Amy M. Trowbridge [b], Henry D. Adams [h]

[a] Department of Geography, Oklahoma State University, Stillwater, OK, USA
[b] Department of Entomology, University of Wisconsin, Madison, WI, USA
[c] Department of Natural Resource Ecology and Management, Oklahoma State University, Stillwater, OK, USA
[d] Agronomy Department, University of Florida, Gainesville, FL, USA
[e] Department of Plant Biology, Ecology, and Evolution, Oklahoma State University, Stillwater, OK, USA
[f] Department of Integrative Biology, Oklahoma State University, Stillwater, OK, USA
[g] Joseph H. Williams Tallgrass Prairie Preserve, The Nature Conservancy, Pawhuska, OK, USA
[h] School of the Environment, Washington State University, Pullman, WA, USA

ARTICLE INFO

Editor: Marie Weiss

Keywords:
Invasive alien species
Airborne remote sensing
Imaging spectroscopy
Lespedeza cuneata
Vegetation functional traits

ABSTRACT

Lespedeza cuneata (sericea lespedeza; hereafter "sericea") is an invasive species brought to the U.S. from East Asia in the 1890s to be used as forage. However, it has now become a growing ecological and economic threat in grasslands of several states in the U.S. southern Great Plains including Oklahoma, Kansas, Missouri, and Nebraska. Here, we demonstrate the capability of airborne imaging spectroscopy to map sericea in a large natural grassland within the Tallgrass Prairie Preserve, the largest protected tallgrass prairie in the world, located in northeastern Oklahoma. Through this research, we investigated which remotely observable vegetation functional traits (referring to biochemical, physiological, and structural traits) contribute to distinguishing sericea from co-occurring native species and whether we can detect sericea remotely through quantifying these functional traits using imaging spectroscopic data (also known as hyperspectral data). To achieve these objectives, full-range airborne hyperspectral data with spatial resolution of 1 m were collected from the study area in August 2020. In addition, a total of 12 vegetation functional traits were measured through field sampling for model development. We first identified functional traits that contributed to separating sericea from other species, and then used them in a classification model to detect sericea in our study site. We found total carotenoids (sum of neoxanthin, violaxanthin, antheraxanthin, zeaxanthin, and lutein), chlorophyll *a* + b (sum of chlorophyll *a* and chlorophyll *b*), total nitrogen, canopy height, potassium, and magnesium as the main functional traits contributing to the detection of sericea; an overall classification accuracy of approximately 94% was reported. However, the proposed approach overestimated sericea cover in species-rich plant communities. Overall, our findings demonstrated an essential role for airborne remote sensing in 1) direct mapping of invasive plants and 2) quantifying functional traits associated with success strategies of invasive species. Eventually, experiments like ours can aid in developing large-scale and science-driven management practices to both identify the current extent, and to control the spread of invasive species in grasslands and similar short-stature environments. This will not only improve management practices but will have major societal and economic benefits.

* Corresponding author.
E-mail address: hamed.gholizadeh@okstate.edu (H. Gholizadeh).
[1] These three authors equally contributed to the paper.

https://doi.org/10.1016/j.rse.2022.112887
Received 25 September 2021; Received in revised form 19 December 2021; Accepted 1 January 2022
Available online 22 January 2022

1. Introduction

1.1. Background

Invasive alien species (IAS) are non-native species that can cause adverse ecosystem and economic effects once introduced (Kettenring and Adams, 2011; Mack et al., 2000). With their rapid expansion, IAS homogenize the flora and fauna of ecosystems and negatively impact ecosystem services (Mooney and Hobbs, 2000; Pejchar and Mooney, 2009). IAS are considered to be the second main cause of global biodiversity loss after habitat destruction (Williamson, 1999). It is estimated that invasive species have caused an economic loss of at least $1.288 trillion (U.S. dollars) worldwide since 1970 (Diagne et al., 2021). IAS are often introduced by humans to habitats outside of their natural range (Hulme, 2009); once introduced, IAS can grow and spread rapidly. Concurrent global changes (e.g., climate, land-use, nutrient cycles) generally promote these biological invasions (Eschtruth and Battles, 2009). However, the impact of global change factors on invasions is spatially complex; while some aspects can promote biological invasions in one region, they might hinder the spread of IAS in other regions (Bradley et al., 2010; Dukes and Mooney, 1999). Given the transboundary and large-scale impacts of IAS, monitoring the spread and studying the mechanisms and strategies of invasions require spatially-explicit approaches. Remote sensing technologies provide the necessary information to develop cost- and time-effective solutions for assessing current and future invasion processes over large geographical extents. In this study, we test how effective remotely sensed data are for detecting IAS in grasslands.

1.2. IAS in grasslands

Grassland ecosystems are threatened by IAS as well as disturbances and land-use change, which in turn can facilitate invasions. Many non-native plants in grasslands were originally introduced for forage production because of their ability to establish and persist in diverse environments, but these are also characteristics that amplify the potential for invasion into unintended ecosystems (Ball et al., 2002). It is paradoxical that most of the characteristics of "good" forage are the same that confer invasiveness and facilitate dominance in diverse plant communities, such as rapid maturation, ability to germinate under a variety of conditions, high seed production, allelopathy, and association with beneficial fungal symbionts. With their rapid expansion, IAS can have negative impacts on grasslands diversity and their capacity to retain existing function and structure in the face of environmental change (Mäkinen et al., 2015; Marquard et al., 2009; Tilman et al., 1997). IAS also reduce forage quality and livestock production of grasslands, lowering economic activity across regions. In the U.S., forage losses alone to IAS are estimated to be approximately $1 billion per year (Pimentel et al., 2001). Given the potential for IAS to have far-reaching negative environmental and economic effects on grasslands, it is critical that we develop operational and cost-effective monitoring systems to understand the status of IAS.

1.3. Remote sensing of IAS in grasslands and short-stature environments

The success of remote sensing techniques at direct mapping of invasive plants, in general, is due to 1) contrasting seasonal phenology of IAS compared to co-occurring native plants, including differences in timing of green-up, flowering, and/or leaf senescence, 2) distinct biochemical, physiological, and structural traits of IAS from native plants, and 3) prevalence of invasive species in the study area (Bolch et al., 2020; He et al., 2015).

The phenology-based approaches use remotely sensed data during time periods in which IAS are spectrally most distinct from native species. For instance, in western California, the invasive *Lepidium latifolium* (pepperweed) was mapped using fine resolution (i.e., small pixel size; 3 m) hyperspectral data during flowering and fruiting when it had distinct spectral response from surrounding green plants (Andrew and Ustin, 2008). Similar remote sensing studies have taken advantage of phenology to map the invasive *Solidago altissima* (Canada goldenrod) early in the growing season (late April) in Japan using fine-resolution hyperspectral data (1.5 m) (Ishii and Washitani, 2013). These phenology-based approaches have also been used for mapping invasive species using coarse-resolution multispectral data. For instance, the invasive *Eragrostis lehmanniana* (Lehmann lovegrass) and *Bromus tectorum* (Cheatgrass) were mapped in southwestern U.S. using MODIS data (Bradley et al., 2018; Huang and Geiger, 2008). While phenology-based IAS detection has shown promising results, its success depends on distinct phenology of target IAS as well as access to remote sensing data with fine temporal resolution.

In addition to phenology, spectral response of plants is affected by their biochemical, physiological, and structural traits. As such, IAS can be remotely detected when they have distinct biochemical, physiological, and structural traits from native plants. For instance, the invasive *Euphorbia esula* (leafy spurge) was detected using imaging spectroscopic data with spatial resolution of 3.5 m (Glenn et al., 2005; Mitchell and Glenn, 2009) presumably because floral bracts of leafy spurge have significantly lower pigment content (chlorophyll a + b and carotenoid) than its leaves (Hunt Jr et al., 2004). Similarly, Yang and Everitt (2010) were able to distinguish *Gutierrezia sarothrae* (Broom snakeweed; an undesirable shrub due to its toxicity to livestock) in Texas rangelands using hyperspectral imagery with fine spatial resolution (1.3 m) due to its erectophile canopy morphology (Everitt et al., 1987). Remote detection of IAS based on their distinct biochemical, physiological, and structural traits is of particular importance in cases where the IAS and co-occurring native species have similar phenology. However, success of these approaches often depends on the availability of hyperspectral data because these data provide the fine spectral resolution necessary for elucidating plant biochemistry and physiology remotely.

Eventually, what makes remote detection of IAS feasible is the abundance of IAS within a plant community (i.e., area covered by IAS) (He et al., 2015). To effectively detect IAS remotely, they need to be the dominant species within a community or form homogeneous patches, large enough to match the spatial resolution of remote sensing observations. Therefore, in addition to temporal and spectral resolution of remotely sensed data, paying specific attention to spatial resolution is warranted if we are to develop operational remote sensing-based IAS monitoring approaches. The role of spatial resolution in detecting IAS in grasslands is particularly significant because 1) grassland IAS often grow in small patches relative to the spatial resolution of common remotely sensed data (e.g., NASA/USGS Landsat-8, ESA Sentinel-2 constellation) and 2) the canopy size of grassland plants is often smaller than the spatial resolution of most remote sensing platforms. In this study, we collected airborne remote sensing data with fine spectral and spatial resolution (pixel size of 1 m) to map the invasive *L. cuneata*, which is a growing threat in grasslands of several states in the U.S.

1.4. The invasive L. cuneata

L. cuneata (commonly known as sericea lespedeza; hereafter "sericea") is a warm-season perennial nitrogen-fixing legume that was brought to the U.S. from East Asia in the 1890s as a cheap forage and for controlling soil erosion (Pieters, 1938; Pieters et al., 1950). Sericea was introduced as a forage species mainly because it is persistent once established. Specifically, sericea is a prolific seed producer, can tolerate drought, reproduces under poor soil conditions (e.g., infertile and acidic soil) and sloping terrain, and is taller than most co-occurring native species and therefore can outcompete other species for light (Brandon et al., 2004; Cline and Silvernail, 1997; Cummings et al., 2007; Donnelly, 1954; Hoveland et al., 1990; Stitt and Clarke, 1941). However, while highly nutritious and palatable early in its development, grazing animals strongly avoid sericea at maturity (Donnelly, 1954; Stitt and

Clarke, 1941). This avoidance is partly due to high concentrations of phenolics, specifically condensed tannins, located throughout the plant that cause gastro-intestinal malaise in many ruminants, including cattle (Donnelly, 1954; Mosjidis et al., 1990; Silanikove et al., 2001). As a result, sericea has become a growing problem in grassland ecosystems and is threatening biodiversity, ecosystem services, and resilience in the face of future environmental change. As of now, the total grassland area invaded by sericea is unknown, in large part due to the difficulty of mapping short-statured invaders of biodiverse grasslands.

Sericea has similar phenology to dominant species in grasslands where it has invaded, with the exception of its green-up and senescence periods. Sericea, anecdotally, starts to green-up about two weeks before other common grassland species and senesces approximately two weeks after native prairie plants. However, this pattern has been reported to vary significantly depending on environmental conditions (e.g., fire regimes, precipitation, temperature) and is likely to shift, albeit with a high level of uncertainty, in response to future global change. Because of comparable phenology of sericea and native species, especially across the broad range of environmental conditions which sericea has invaded, we posit that identifying sericea using its distinct biochemical, physiological, and structural traits instead of those based on phenology may result in more accurate remote detection of this IAS.

This paper seeks to fill a critical knowledge gap that moves beyond a reliance on phenology alone towards using vegetation functional traits for remote detection of IAS in natural grasslands. Specifically, we addressed two objectives: 1) determine remotely observable vegetation functional traits—focusing specifically on biochemical, physiological, and structural traits—that distinguish sericea from co-occurring native species and 2) use these functional traits to develop a robust method for detecting the extent of sericea invasions. To achieve these objectives, we collected airborne imaging spectroscopic data with fine spatial resolution (1 m) as well as a suite of vegetation functional traits from The Nature Conservancy's Tallgrass Prairie Preserve (TGPP; also known as the Joseph H. Williams Tallgrass Prairie Preserve), a large natural grassland ecosystem located in northeastern Oklahoma. Our central hypothesis was that sericea has specific functional traits (e.g., higher total nitrogen content, large canopy height) that can be used to distinguish it from co-occurring native species in remotely sensed data. We based our central hypothesis upon the fact that depending on their functional traits, plants can display different spectral signatures in remotely sensed data (Ustin and Gamon, 2010). We are not aware of any other research that has delineated spatial distribution of IAS in grasslands through direct quantification of vegetation functional traits using remotely sensed data. This work helps us 1) identify the underlying functional traits that distinguish sericea from native species and 2) fill knowledge gaps surrounding remote detection of IAS in grasslands and similar short-stature environments, where direct detection of IAS is deemed challenging because of scale mismatch between spatial resolution of remotely sensed data and plant size.

2. Methods

2.1. Study site

The study was conducted in northeastern Oklahoma at TGPP (36° 50′ N, 96° 25′ W) which is the largest protected tallgrass prairie on Earth (Coppedge et al., 1998; TNC, 2021). TGPP is managed using synergistic application of prescribed fire and grazing with the goal of generating structural heterogeneity that is critical to grassland biodiversity conservation (Fuhlendorf and Engle, 2004; Fuhlendorf et al., 2009). We limited our experiment to the northern portion of TGPP with a total area of 47 km^2 (approximately one-third of TGPP's total area; Fig. 1). In this part of TGPP, about one-third of pastures are burned annually, and cattle freely graze throughout. Approximately 90% of TGPP is covered with tallgrass species, such as little bluestem (*Schizachyrium scoparium*), big bluestem (*Andropogon gerardii*), Indian grass (*Sorghastrum nutans*), and switchgrass (*Panicum virgatum*), with the remaining land-cover being oak woodland (Hamilton, 2007). Average summer high temperature and winter low temperature are 32 °C and 3 °C, respectively. Average annual precipitation at TGPP is approximately 960 mm (Sherrill, 2019).

Sericea invasion is a growing threat at TGPP. Previous work based on two field-based species inventories has reported 9% increase in sericea percent cover at TGPP from 1997 (near zero sericea cover) to 2018 (approximately 9% sericea cover; Sherrill, 2019). As a result, The Nature Conservancy has spent over $1.3 million and more than 25,000 person-hours between 1997 and 2019 to control the spread of sericea through

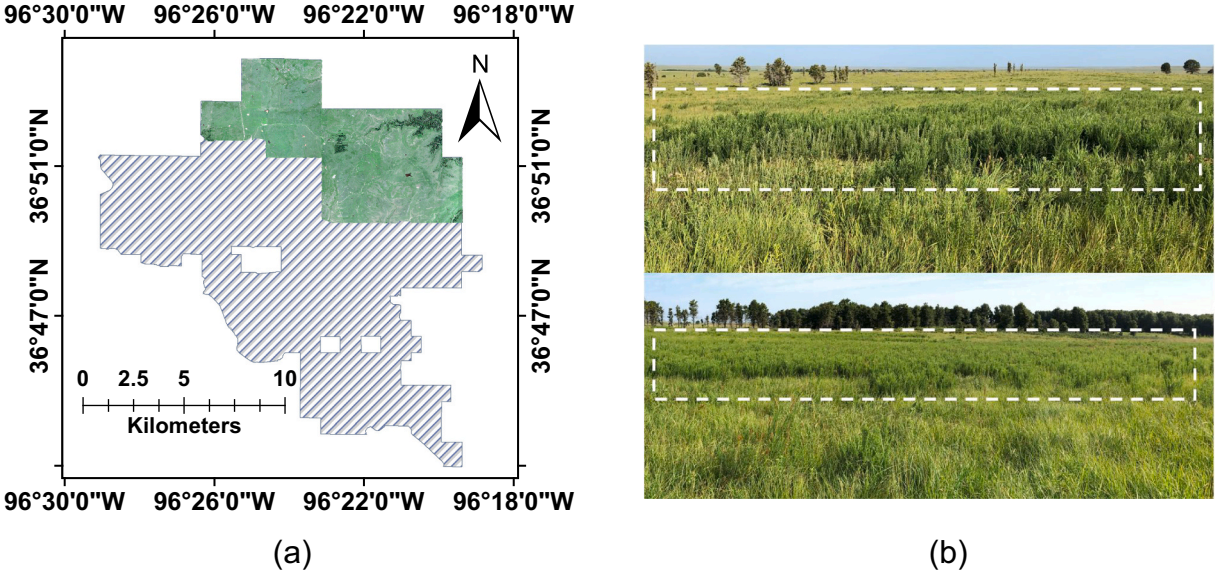

Fig. 1. (a) The study area within The Nature Conservancy's Tallgrass Prairie Preserve (TGPP; also known as Joseph H. Williams Tallgrass Prairie Preserve) is shown with a true colour composite (date of imagery: August 03, 2020). This portion of TGPP is managed with fire-cattle grazing while the cross-hatched regions are managed by fire-bison grazing. (b) Homogeneous patches of sericea are shown inside dashed white rectangles. Sericea patches are often taller and denser than their neighboring co-occurring native species at TGPP (date of photos: August 8, 2020). Sericea does not necessarily always occur in large and homogeneous patches (similar to Fig. 1b); it can also occur in low abundance mixed with co-occurring native species (see Fig. S1 in Supplementary material).

application of herbicide (e.g., metsulfuron-methyl and triclopyr) coupled with management through fire and grazing.

2.2. Collecting ground reference data for image classification

We collected three data sets for developing and testing our models. We will refer to these as (1) homogenous training data set ($n = 49$), (2) homogenous validation data set ($n = 78$), and (3) heterogeneous validation data set ($n = 133$). Briefly, the homogenous training data set included 49 homogeneous grassland "patches" and was used for developing models, the homogenous validation data set included 78 homogeneous grassland "patches" and was used for model validation, and the heterogeneous validation data set included 133 60 m × 60 m heterogeneous and diverse grassland "plots" and was used for model validation.

2.2.1. Collecting ground reference data for classification training

We identified 49 grassland "patches" at TGPP for model development and trait sampling between late July and early August 2020. We selected grassland patches that were dominated by sericea as well as those that were free of sericea. A patch was labeled sericea if the observed sericea canopy cover was more than 75% and a patch was labeled non-sericea if the observed sericea canopy cover was approximately 0%. All non-sericea patches were homogeneous and covered with dominant species at TGPP. Specifically, these non-sericea patches did not include more than three dominant species; percent cover of each species in non-sericea patches was determined visually.

In our homogenous training data set, 20 patches were dominated by sericea (i.e., recorded as "sericea") and the remaining 29 patches were non-sericea (i.e., native species). Since our ultimate goal was mapping sericea, this binary sericea vs. non-sericea approach was justifiable. We recorded the area of these patches using a GPS unit (Trimble GeoXH, Trimble, Sunnyvale, CA, USA) and applied differential GPS correction in the GPS Pathfinder Office software v5.90 (Trimble, Sunnyvale, CA, USA) to minimize uncertainty associated with GPS measurements and improve location accuracy to 1–3 m. Area of these patches ranged from approximately 19 m^2 to 855 m^2, with an average area of 298 ± 182 m^2 (mean ± standard deviation). We chose to use this patch-level approach, rather than a point-to-pixel approach that would link one individual plant to a single pixel in airborne remotely-sensed data, to minimize risk of mismatch between field sampling points and remotely-sensed pixels. Given the small size of plants in our grassland, even a slight positional mismatch of 10–20 cm, could have translated into assigning functional traits of one species (e.g., sericea) to the image spectrum of another species (for example, see Fig. S1 in Supplementary material).

2.2.2. Collecting ground reference data for classification validation

Although we used homogeneous patches of sericea to develop classification models, IAS do not necessarily always grow in large patches similar to Fig. 1b; they can also occur in low abundance mixed with co-occurring native species (see Fig. S1 in Supplementary material). To test the capability of remote sensing models for detecting sericea in both cases, we collected two validation data sets. Specifically, we collected one independent homogenous validation data set to assess model performance at detecting homogeneous patches of sericea and one heterogeneous validation data set to determine how accurately our model estimated actual sericea percent cover in species-rich plant communities.

For our homogenous validation data set, we identified 78 grassland "patches" at TGPP in late July 2020. Out of 78 patches, 36 patches were sericea and the remaining 42 patches were non-sericea. We applied the same criteria used for selecting patches in our homogenous training data set (described in Section 2.2.1) to identify patches for our homogenous validation data set. We recorded the extent of these patches using a GPS unit (Trimble GeoXH, Trimble, Sunnyvale, CA, USA) and differentially corrected GPS coordinates. Minimum and maximum area of these validation patches were approximately 11 m^2 and 1139 m^2, respectively, with an average area of 175 ± 166 m^2 (mean ± standard deviation).

For our heterogeneous validation data set, we collected sericea abundance data at 133 equal-sized grassland "plots" in July–August 2020. These validation plots were approximately 60 m × 60 m in size. Sericea percent cover was documented every five meters along two perpendicular 60 m transects within each plot using a 50 cm × 20 cm quadrat. Overall, we collected sericea percent cover at 25 50 cm × 20 cm quadrats within each plot and 3325 quadrats in total (Fig. S2 in Supplementary material). Endpoints of each transect were measured using a handheld GPS unit (Trimble Juno 3B, Trimble, Sunnyvale, CA, USA) and differentially corrected afterwards. This validation data set was representative of communities with high plant diversity; the average species richness within these plots was approximately 29.

2.3. Collecting foliage samples for quantifying vegetation functional traits

We sampled a total of 193 plants from our 49 patches in the homogenous training data set. Specifically, we selected sunlit top-of-canopy foliage from 69 sericea and 124 non-sericea canopies. These samples were used to quantify 12 vegetation functional traits, including total nitrogen (TN, %), chlorophyll *a* + b (Chl a + b; mg/g), total carotenoids (Car; μg/g), total phenolic content (TPC; mg/g), phosphorus (P; %), calcium (Ca; %), potassium (K; %), magnesium (Mg; %), iron (Fe; ppm), zinc (Zn; %), leaf mass per area (LMA, g/m^2), and canopy height (cm). We selected functional traits that are relevant for plant and ecosystem function, including light capture and growth (TN, Chl a + b, Car), photoprotection (Car), chemical defense and grazing animals' diet preference (TPC), metabolic processes and micro- and macronutrients (P, Ca, K, Mg, Fe, Zn), and vegetation structure (LMA, canopy height).

We quantified TN with a combustion analyzer (Leco CN628, LECO Corporation, St. Joseph, Michigan, USA) using 0.15 g of each foliage sample at The Soil, Water, and Forage Analytical Laboratory (SWFAL), Oklahoma State University. We analyzed mass-based Chl a + b, Car, and TPC at The Forest Entomology Lab, University of Wisconsin-Madison. For Chl a + b (sum of chlorophyll *a* and chlorophyll *b*), Car (sum of neoxanthin, violaxanthin, antheraxanthin, zeaxanthin, and lutein), and TPC quantification, foliage samples were immediately frozen in liquid nitrogen, and stored on dry ice in the field until they could be transferred to a -80 °C freezer. Chl a + b and Car were quantified using High-Performance Liquid Chromatography (HPLC; Agilent 1200 Series, Agilent Technologies, Santa Clara, CA). The HPLC system included a 150 mm × 4.6 mm column with 2.7 μm particle size (Poroshell EC-120 C18, Agilent InfinityLab, Agilent Technologies, Santa Clara, CA). Chl a + b and Car were extracted by sonicating 0.1 g of ground tissue in 0.5 mL of ice-cold acetone for ten minutes, after which 1 mL of ice cold EtOH containing 0.1% butylated hydroxyanisole was added, and the mixture was sonicated for five minutes. Samples were then centrifuged for five minutes at 10,000 r.p.m. at 4 °C. This extraction was repeated twice, the supernatants were pooled, and solvents were evaporated under a stream of N. Residue was resuspended in 1 mL of Acetonitrile:Methanol:Tris8.0 (76:17:7; Solvent A). Methanol:Hexane (4:1) was used as solvent B. For each sample, 20 μL of pigment extract was injected and the flow was set to 0.8 mL/min. Concentrations of chlorophyll *a* and chlorophyll *b* were quantified based on their absorbance at 432 and 466 nm, respectively. To determine concentration of Car (i.e., neoxanthin, violaxanthin, antheraxanthin, zeaxanthin, and lutein), absorbance at 445 nm was used. Quantification of neoxanthin, violaxanthin, antheraxanthin, zeaxanthin was based on the normalized coefficients provided in De Las Rivas et al. (1989). For TPC, 0.1 g of ground tissue was extracted in 1 mL of MeOH for 24 h. The supernatants were decanted and the samples were centrifuged for five minutes at 12,000 r.p.m. Next, 25 μL of each sample extract was added to 50 μL of 10% Folin-Ciocalteau reagent (Ainsworth and Gillespie, 2007) and 200 μL of 1 M $NaHCO_3$ was added to each tube. The mixture was then incubated at room temperature on an orbital

shaker at 150 r.p.m. for 60 min. TPC was quantified in Gallic Acid Equivalents (GAE) relative to gallic acid standard curve. We quantified P, Ca, K, Mg, F, and Zn from 0.5 g of dry leaf tissue after digestion in 10 mL of nitric acid at 120 °C for 2 h using an Inductively Coupled Plasma device (ICP; Spectro Arcos II, SPECTRO Analytical Instruments GmbH, Kleve, Germany) at the SWFAL lab. Foliage samples for LMA measurements were first weighed in the field, stored in humidified bags, and kept on ice to prevent wilting during transport to The Environmental Ecology Lab at Oklahoma State University. To calculate LMA, we first scanned leaves on a flatbed scanner (Canon CanoScan 4400, Canon, Tokyo, Japan). Then, leaf area was quantified from images using 'leafarea' package (Katabuchi, 2015) in R (R Core Team; www.r-project.org). After scanning, samples were oven-dried at 65 °C for 48 h before recording dry mass. We calculated LMA as leaf dry mass (g) divided by leaf area (m^2). Finally, we measured canopy height at each foliage sampling location within each grassland patch in the homogenous training data set using a visual obstruction technique (Limb et al., 2007). Specifically, a 1 m × 1 m whiteboard was placed vertically at each foliage sampling location and an RGB image was taken with the whiteboard in the background (see Fig. S3 in Supplementary material for an example). We took a total of 193 images using an RGB digital camera (Fuji FinePix XP135, Fujifilm, Tokyo, Japan). Through setting an image threshold, vegetation pixels were separated from the 1 m × 1 m whiteboard background and vegetation height was determined.

2.4. Spectral data collection

2.4.1. Leaf-level spectral sampling

We collected leaf-level spectra in the field within the 350–2500 nm range using an ASD FieldSpec 3 spectroradiometer equipped with a contact leaf probe (Malvern Panalytical, Malvern, UK; Fig. 2a). Data were acquired between late July and early August 2020 simultaneously with our vegetation functional trait sampling. Three sets of foliage samples from the same plants that were used for functional trait sampling were selected and their leaf-level spectral reflectance signatures were measured. Each spectrum was the average of 100 readings. The average spectrum obtained from these three samples was used as the final leaf-level spectral signature. The spectroradiometer was warmed-up in the field for 45 min before each data collection campaign, calibrated for dark current, and referenced to a white calibration panel (Labsphere, North Sutton, NH, USA) every 15 min.

2.4.2. Airborne data collection for canopy-level spectral sampling

We collected full-range airborne hyperspectral data from TGPP. Data collection started at 10:07 am (15:07 GMT) and ended before solar noon at 12:42 pm local time (17:42 GMT), on August 03, 2020 using a Twin Commander 500-B aircraft (Aero Commander, Oklahoma City, OK). A total of 21 flight lines were collected using a pushbroom imaging spectrometer (AISA Fenix 1 k, Specim, Oulu, Finland). The sensor covers 400–2450 nm range in 323 bands with spectral resolution of approximately 4.5 nm in the 400–970 nm range and 14 nm in the 970–2450 nm range. The airborne imager had 1024 spatial pixels and field of view was 40°. Flight altitude of the aircraft was approximately 1400 m above ground level and the resulting data had spatial resolution (i.e., pixel size) of 1 m. To improve the positional accuracy of airborne data, real-time kinematic Global Navigation Satellite System (GNSS) corrections were used, hyperspectral sensor and the navigation system of the aircraft were boresight-calibrated, and 1 m digital elevation model (DEM; from USGS 3DEP) was used for ortho-correction of hyperspectral data. Finally, all radiance images were converted to reflectance using ATCOR-4 (Richter and Schläpfer, 2002), which uses MODTRAN-5 radiative transfer model (Berk et al., 2006). After removing the noisy and water vapor absorption bands, the final airborne data set had 238 bands covering 431.10–1299.36 nm, 1487.71–1775.03 nm, and 1998.23–2353.76 nm wavelengths (Fig. 2b).

2.5. Data analysis

Our approach had four main steps. Briefly, step 1 included identifying vegetation functional traits that distinguished sericea from co-occurring native species using traits measured in the field. In step 2, we developed partial least squares regression (PLSR; Wold et al., 2001) models and applied them to airborne hyperspectral data to estimate functional traits identified in step 1 throughout our study area. In step 3, we used raster layers of vegetation functional traits generated in the previous step and developed partial least squares linear discriminant analysis (PLS-LDA) classification (Barker and Rayens, 2003; Brereton, 2009) to separate sericea from co-occurring native species. Finally, step 4 focused on classification accuracy assessment using two independent validation data sets. Detailed descriptions of all the analysis steps are discussed below. In addition, a schematic diagram of our approach is illustrated in Fig. 3.

2.5.1. Determining vegetation functional traits that distinguish sericea from co-occurring native species

We used Kruskal-Wallis test (non-parametric version of ANOVA) (Kruskal and Wallis, 1952) to assess the difference between sericea and non-sericea species for each functional trait individually. We applied this test to 12 functional traits measured from 193 foliage samples in our homogenous training data set.

This statistical test does not consider the synergetic effect of vegetation functional traits at separating sericea from non-sericea species (i.e., when the combined effect of two or more vegetation functional traits is greater than the sum of independent individual effects). Therefore, to identify vegetation functional traits that contributed to distinguishing sericea from native species (we refer to these functional traits as "important traits"), we used PLS-LDA classification approach coupled with conditional synergetic score (COSS) (Li et al., 2010). COSS

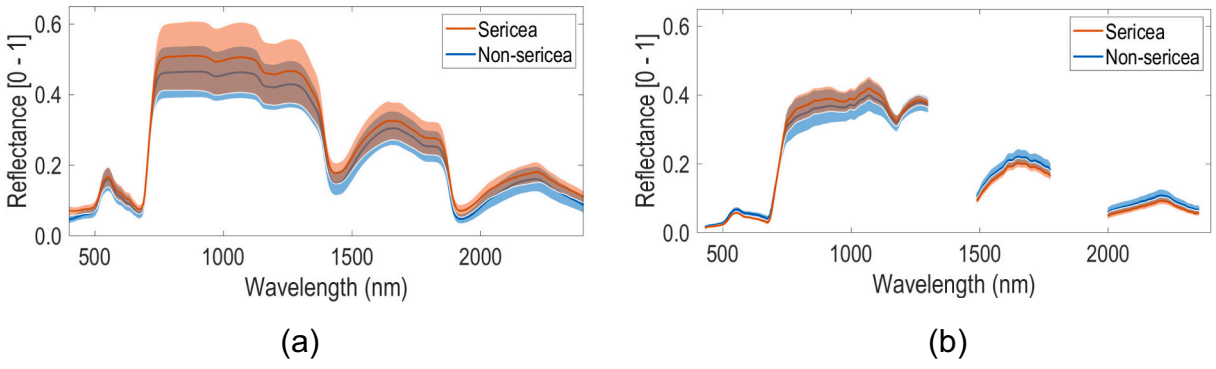

Fig. 2. (a) Average reflectance of sericea leaves vs. non-sericea leaves from leaf-level ASD data and (b) average reflectance of sericea patches vs. non-sericea patches from airborne data. Missing wavelength regions in the airborne data are water vapor absorption bands. Shaded regions show ±1 standard deviation of spectra.

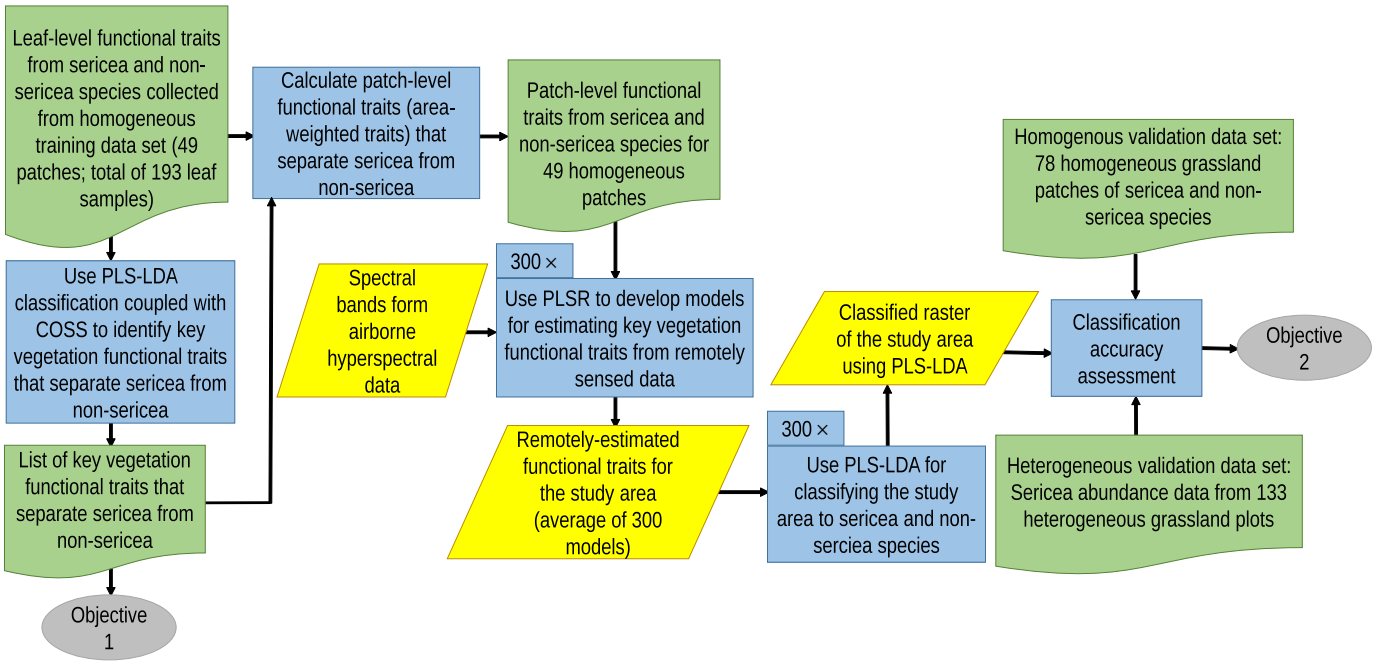

Fig. 3. Schematic diagram illustrating analysis steps in our study. While this diagram shows the main analyses and objectives, detailed data processing steps are described in Section 2.5. In this flowchart, blue rectangles represent processing steps (e.g., partial least squares regression), yellow parallelograms represent remote sensing data products (e.g., remotely-estimated vegetation functional traits), and green rectangles with wavy base represent other input/output data (e.g., validation data). (For interpretation of the references to colour in this figure legend, the reader is referred to the web version of this article.)

estimates the importance of each variable while taking into account the effect of all other variables. Standardized (i.e., centered and scaled) leaf-level vegetation functional traits were inputs and class labels (i.e., sericea and non-sericea) were PLS-LDA outputs.

Specifically, we selected a random subset of training data points (50% of 193 foliage samples), developed PLS-LDA models (Fig. 3) with and without the i^{th} trait (out of 12 vegetation functional traits), estimated classification mean prediction error of each model using the remaining 50% of the data points, and calculated COSS. COSS was defined as $-\log_{10}(p)$, where p is the Mann-Whitney U test p-value of the difference between mean prediction errors of two models: a model including all vegetation functional traits and a model with one of the vegetation functional traits permuted. A COSS threshold value of 2, which corresponds to p-val of 0.01, was considered and all vegetation functional traits with COSS $\geq$2 were deemed important in separating sericea from non-sericea.

2.5.2. Scaling leaf-level traits to patch-level

To develop models for remote detection of sericea in airborne hyperspectral data, we needed to quantify vegetation functional traits at a patch-level. Because sampling and quantifying functional traits for all leaves in each patch was not feasible, we used the average of leaf-level traits within each patch in our homogenous training data set. For canopy height, we took the average of vegetation height in each patch—measured through the visual obstruction technique. For patches that were composed of more than one species, we weighted leaf-level traits by field-measured species percent cover. Since patches in our training data set were homogeneous and did not include more than three dominant species, we assumed that this area-based scaling approach had comparable performance to other weighting approaches, such as those based on relative biomass (Wang et al., 2019).

2.5.3. Developing PLSR models for mapping important functional traits using spectral data

We used PLSR to estimate the values of important vegetation functional traits from spectral data (Asner and Martin, 2009; Serbin and Townsend, 2020; Singh and Glenn, 2009; Wang et al., 2020; Wold et al., 2001). Specifically, we developed PLSR models at both leaf- and patch-level using the data collected from 49 patches in our homogenous training data set. While the patch-level PLSR models were applied to airborne spectral data to estimate vegetation functional traits throughout the study area, leaf-level PLSR models were developed solely for the purpose of evaluating the performance of our patch-level PLSR models and were not used for further analysis.

For leaf-level PLSR models, we used the vector-normalized reflectance data from the ASD FieldSpec 3 spectroradiometer as the independent variables (or input; Fig. S4a in Supplementary material)—where reflectance in each wavelength is divided by the full-spectrum's l^2-norm (Feilhauer et al., 2010)—and important functional traits as the dependent variables (or output). We used 50% of traits from 193 foliage samples and the corresponding spectra for developing PLSR models and the remaining data points for testing. We developed separate PLSR models for each important trait and repeated this process 300 times (Fig. 3) through randomized permutations to estimate uncertainty in our trait retrievals (Singh et al., 2015). Optimum number of PLSR components were determined based on cross-validated mean squared prediction error.

For our patch-level PLSR models, we used the average vector-normalized reflectance spectra of each patch from airborne data (except for noisy and water vapor absorption bands) as the independent variables (Fig. S4b in Supplementary material) and scaled patch-level traits from Section 2.5.2 as the dependent variables. We then repeated the same process that we used for developing our leaf-level PLSR models as described above; each important vegetation functional trait was estimated 300 times throughout the study area by applying 300 patch-level PLSR models to airborne hyperspectral data. To implement PLSR, the "plsregress" command in (MATLAB, 2020) was used (MathWorks Inc., Natick, Massachusetts, USA).

2.5.4. Mapping sericea invasion using airborne data

After determining important vegetation functional traits that separated sericea from co-occurring native species (Section 2.5.1) and

estimating the values of important vegetation functional traits throughout the study area by applying PLSR models to airborne data (Section 2.5.3), we developed PLS-LDA classification models for mapping sericea in our study area.

Inputs for PLS-LDA classification were raster layers of average vegetation functional traits estimated from 300 PLSR models that were developed in Section 2.5.3 (one raster layer for each important trait) and the outputs were class labels (sericea vs. non-sericea). We used the homogenous training data set for training the PLS-LDA classification model, where each patch was considered as one data point. In other words, each patch was represented by the vector of important traits as classification input and one label as classification output. We developed 300 PLS-LDA models using a leave-25%-out approach iterated 300 times. Specifically, we selected a random subsample comprised of 75% of training patches from our homogenous training data set, developed a PLS-LDA model for each subsample, and repeated this process 300 times. We developed 300 PLS-LDA models, instead of one model, to have a more reliable assessment of accuracy (or uncertainty) as described below.

2.5.5. Classification accuracy assessment

We used two independent validation data sets to assess the performance of our IAS detection approach as described in Section 2.2.2. The homogenous validation data set included 78 patches of sericea and co-occurring native species. We used this data set to assess classification accuracy in terms of overall accuracy, producer's accuracy (=100%-omission error), user's accuracy (=100%-commission error), and kappa statistic (Cohen, 1960; Rosenfield and Fitzpatrick-Lins, 1986) obtained from our 300 PLS-LDA models.

The heterogeneous validation data set included sericea percent cover measured at 133 heterogeneous grassland plots. PLS-LDA-estimated abundance of sericea within sampling plots were compared to observed sericea abundance in terms of proportion of explained variance (R^2), root mean square error (RMSE), and normalized RMSE (NRMSE).

2.5.6. Determining spectral regions in airborne data that separated sericea from native species

Finally, we also identified spectral bands in our airborne data that contributed to detecting sericea. To achieve this goal, we evaluated the relative importance of each spectral band in the airborne data at separating sericea from co-occurring native species using COSS analysis, similar to what we used in Section 2.5.1. For this analysis, we used spectral bands from airborne data (except for noisy and water vapor absorption bands) as inputs; we also used class labels (i.e., sericea and non-sericea) from 49 patches in the homogenous training data set as outputs. Following this approach, we assigned COSS scores to spectral bands to determine the relative contribution of each band at detecting sericea.

3. Results

3.1. Vegetation functional traits—sericea vs. other species

Statistical analysis based on Kruskal-Wallis test showed that sericea had significantly higher TN, Chl a + b, Car (and Chl a + b/Car ratio; see Fig. S5 in Supplementary material), TPC, and canopy height than other species at $\alpha = 0.05$, while it had significantly lower K, Mg, and Fe content compared to other species (Fig. 4). The difference between sericea and non-sericea species was not significant for the remaining functional traits (P, Ca, Zn, and LMA). Results also showed that, in general, the range and variation of functional trait values for non-sericea patches were larger than sericea patches. This was expected as our non-

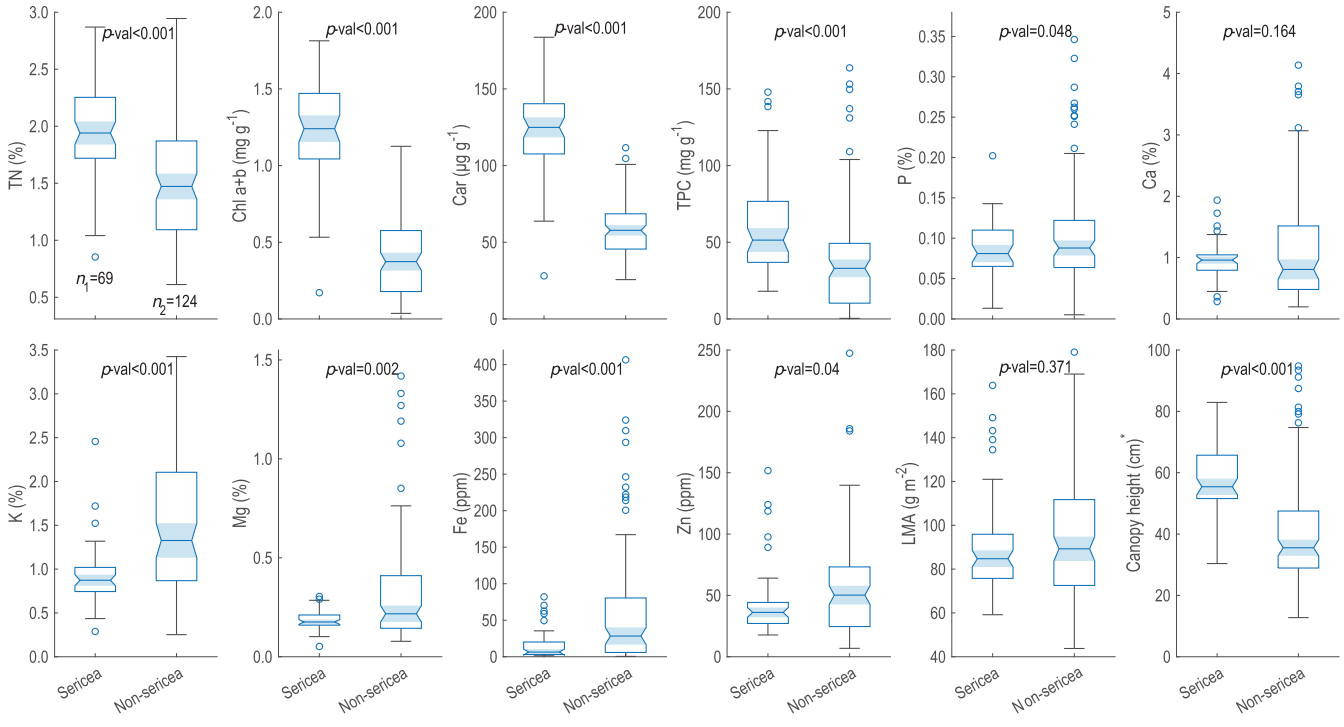

Fig. 4. Leaf-level functional traits (69 sericea and 124 non-sericea foliage samples). We used Kruskal-Wallis test to assess differences between sericea and non-sericea leaves. Functional trait acronyms: TN: total nitrogen, Chl a + b: Chlorophyll a + b, Car: total carotenoids (sum of neoxanthin, violaxanthin, antheraxanthin, zeaxanthin, and lutein), TPC: total phenolic content, P: phosphorus, Ca: calcium, K: potassium, Mg: magnesium, Fe: iron, Zn: zinc, and LMA: leaf mass per area. In each boxplot, the central box indicates the middle 50% of the data (between 25th and 75th percentile), the blue horizontal line inside each box represents the data median, the whiskers indicate the remaining data points excluding outliers, and data points beyond the whiskers show outliers. *All traits, except canopy height, were measured at leaf-level; we measured canopy height at each foliage sampling location within our training patches using the visual obstruction technique. (For interpretation of the references to colour in this figure legend, the reader is referred to the web version of this article.)

sericea category included several species from different functional groups, such as graminoids and woody shrubs, which can potentially result in large inter-species trait variability.

COSS scores were used to estimate the importance of each vegetation functional trait in separating sericea from non-sericea species. COSS scores estimated from leaf-level functional traits identified Car, Chl a + b, TN, canopy height, K, and Mg as the most important functional traits for separating sericea from non-sericea species (Fig. 5).

3.2. Estimating vegetation functional traits from spectral data using PLSR

After identifying important vegetation functional traits (i.e., Car, Chl a + b, TN, canopy height, K, and Mg), we used PLSR to estimate them using leaf-level and airborne spectral data (Fig. 3). Although the relationships between measured and PLSR-predicted functional traits were significant at both leaf- and patch-level (i.e., estimated from airborne imagery) for $\alpha = 0.05$, PLSR model performance was not the same for all functional traits (Fig. 6).

For leaf-level data points (Fig. 6a, c, e, g, i), model performance, expressed as R^2, ranged from 0.42 ± 0.06 (mean ± 1 standard deviation of 300 permutations; p-val < 0.001) for TN (Fig. 6a) to 0.63 ± 0.06 (p-val < 0.001) for K (Fig. 6g). In terms of prediction error, Car had the highest error rate (NRMSE of 19.26 ± 2.20%; Fig. 6e) and K had the lowest error rate (NRMSE of 15.09 ± 2.18%; Fig. 6g).

After scaling up functional traits to patch-level based on percent cover (as described in Section 2.5.2), PLSR models were developed to link scaled traits to airborne spectra (Fig. 6b, d, f, h, j, k). Chl a + b and Car PLSR models showed the weakest predictive performance at patch-level with R^2 of 0.32 ± 0.10 (p-val < 0.001; Fig. 6d) and 0.34 ± 0.09 (p-val < 0.001; Fig. 6f), respectively. PLSR-predicted canopy height and K showed the strongest agreement with the observed data at patch-level with R^2 of 0.57 ± 0.13 (p-val < 0.001; Fig. 6k) and 0.51 ± 0.12 (p-val < 0.001; Fig. 6h), respectively.

Our results showed that although the performance of patch-level PLSR models, in general, weakened after scaling up, these models had comparable performance to those obtained from leaf-level data. This comparable performance indicated the potential of area-based trait upscaling when sampling functional traits from large number of individuals is not feasible. Overall, based on PLSR results, sericea leaves and sericea-dominated patches consistently showed significantly higher Car, Chl a + b, TN, and canopy height values but lower K and Mg.

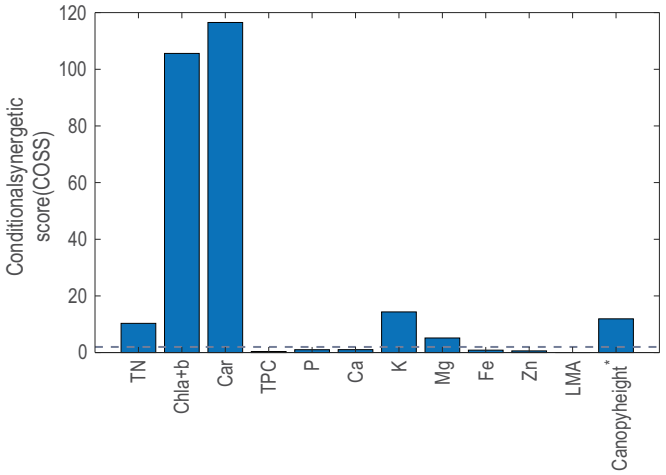

Fig. 5. COSS scores showing the importance of each vegetation functional trait in separating sericea from non-sericea species. Dashed line shows cutoff COSS value of 2. Functional traits with COSS values greater than 2 are considered important. Functional trait acronyms: TN: total nitrogen, Chl a + b: Chlorophyll a + b, Car: total carotenoids, TPC: total phenolic content, P: phosphorus, Ca: calcium, K: potassium, Mg: magnesium, Fe: iron, Zn: zinc, and LMA: leaf mass per area. Note: standardized (i.e., centered and scaled) vegetation functional traits were used in the analysis. *All traits, except canopy height, were measured at leaf-level; we measured canopy height at each foliage sampling location within our training patches using the visual obstruction technique.

PLSR coefficients at both leaf-level and patch-level (i.e., airborne imagery) showed that wavelengths contributing to the prediction of functional traits (i.e., those wavelengths with coefficients deviating from zero) were distributed across different regions of the electromagnetic spectrum (Fig. 7; Fig. S6 in Supplementary material). Some of these wavelength features aligned well with the known absorption features of a number of selected key traits (Fig. 5). Notable was the contribution of bands within the visible region of the spectrum which are associated with the absorption features of Chl a + b and Car (Curran, 1989; Wang et al., 2020; see also Section 4.2 for further discussion of the linkages between key traits and key spectral bands).

3.3. Sericea mapping using remotely-estimated vegetation functional traits

3.3.1. Sericea presence/absence mapping accuracy assessment

To assess the performance of PLS-LDA approach at detecting sericea absence/presence, an independent validation data set consisting of 78 grassland patches was collected (the homogenous validation data set as described in Section 2.2.2; Fig. 3). Results obtained from this validation data set reported an overall classification accuracy of 94.0 ± 2.0% (mean ± 1 standard deviation obtained from 300 PLS-LDA models) indicating that PLS-LDA classifier correctly classified a patch with the probability of approximately 94% (Table 1). Kappa coefficient was 0.87 ± 0.04 indicating a very strong agreement between classified data and reference validation data (Landis and Koch, 1977). Producer's accuracy for sericea and non-sericea classes were 91.5 ± 4.8% and 96.2 ± 2.2%, respectively, indicating the percentage of ground truth patches in each class that were correctly labeled (e.g., approximately 92% of sericea ground truth patches were classified correctly). User's accuracy was reported to be 95.5 ± 2.4% and 93.1 ± 3.5% for sericea and non-sericea classes, respectively. User's accuracy values showed the percentage of classified patches in each class that were correctly labeled (e.g., approximately 96% of patches labeled as sericea in the final product were classified correctly).

3.3.2. Sericea abundance estimation accuracy assessment

PLS-LDA classification was also used to estimate sericea abundance fraction at our heterogeneous validation data set, where sericea was rarely the dominant species (Fig. 3). Minimum and maximum measured sericea percent cover in these validation "plots" were approximately 0% and 57.5%, respectively. There was a strong agreement between measured and estimated sericea abundance fraction in our validation plots with an R^2 of 0.66 (p-val < 0.001; Fig. 8). Model RMSE and NRMSE values were 0.07 and 12.69%, respectively. Although there was a significantly strong relationship between measured and estimated sericea abundance fraction, the PLS-LDA approach overestimated sericea abundance. Furthermore, the developed regression model was driven by a few data points (i.e., plots) with high sericea percent cover.

Finally, sericea invasion within the study area was mapped by applying the 300 PLS-LDA models to the airborne imagery (Fig. 9a). A pixel was considered sericea if it was classified as sericea in all 300 PLS-LDA models. This mapping analysis reported that about 10% of the study area was dominated by sericea (Fig. 9b).

3.4. Contribution of different bands at separating sericea from non-sericea species in airborne imagery

COSS scores were used to estimate the relative contribution of each spectral band to sericea detection in airborne data (Fig. 10). Considering a threshold value of 2, out of 238 bands in our airborne data, 66 bands were deemed important in separating sericea from non-sericea species. COSS analysis pointed to greater contribution of bands within the visible

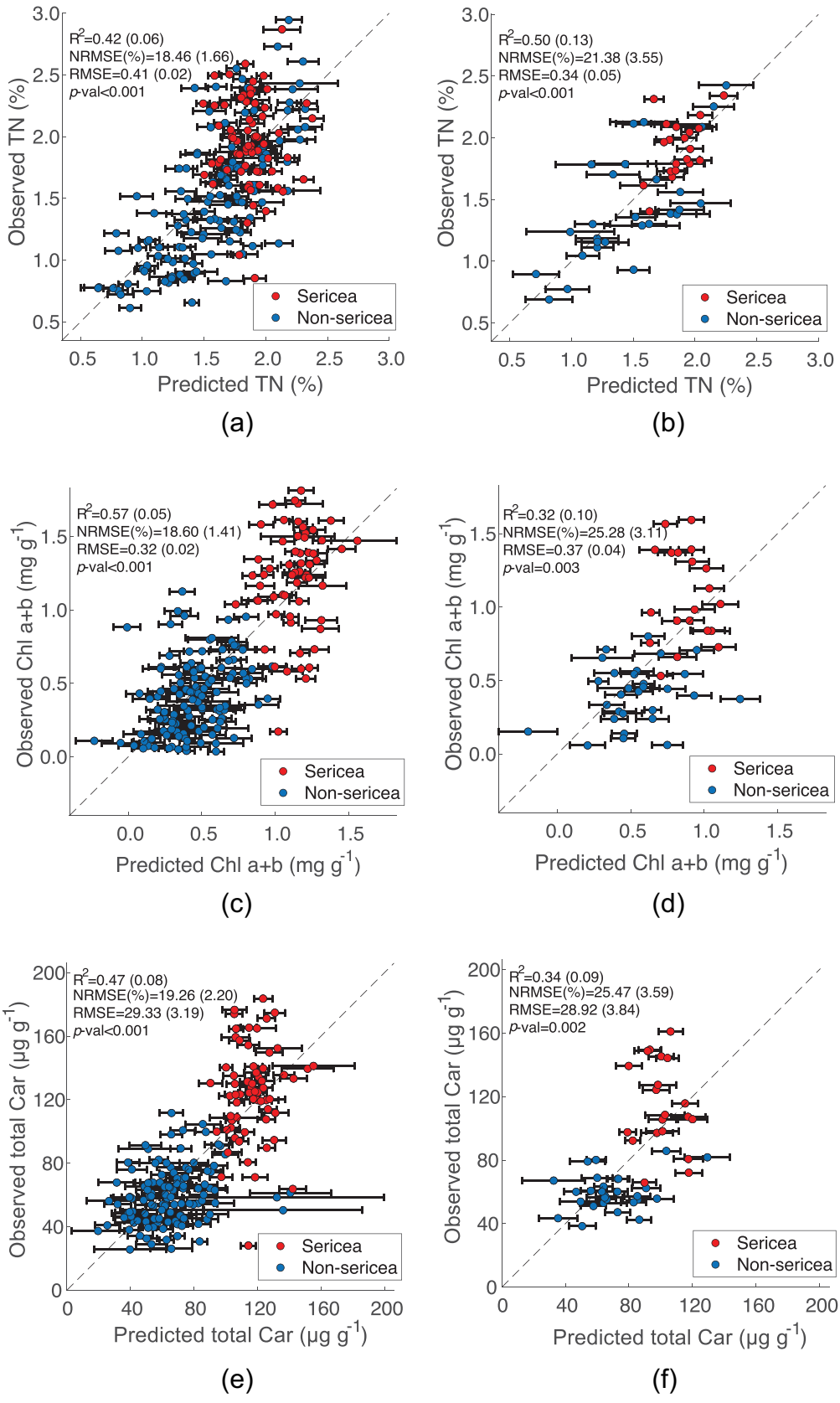

Fig. 6. Predicted vs. observed functional traits. (a, c, e, g, i) In these PLSR models, independent variables are vector-normalized leaf-level ASD reflectance data and dependent variables are leaf-level functional traits. (b, d, f, h, j) Independent variables are vector-normalized airborne reflectance data and dependent variables are scaled-up patch-level functional traits. (k) For canopy height, only patch-level results obtained from airborne data are shown. For these PLSR models, all spectral bands (except for noisy and water vapor absorption bands) were used. Horizontal bars show ±1 standard deviation from 300 permutations. NRSME: normalized RMSE in percent; numbers inside parentheses show standard deviation from 300 permutations; *p*-val is the median *p*-val of 300 permutations. Dashed lines are 1:1 lines. Functional trait acronyms: TN: total nitrogen, Chl a + b: Chlorophyll a + b, Car: total carotenoids, K: potassium, and Mg: magnesium.

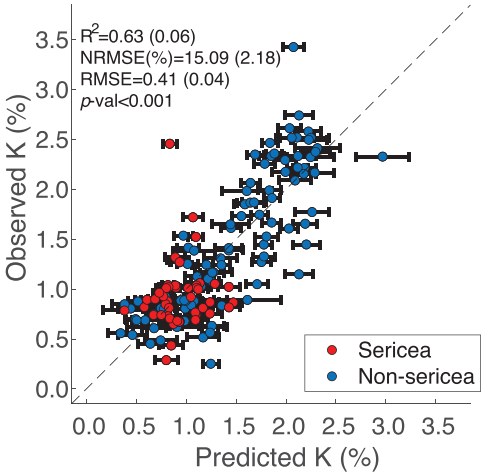

(g)

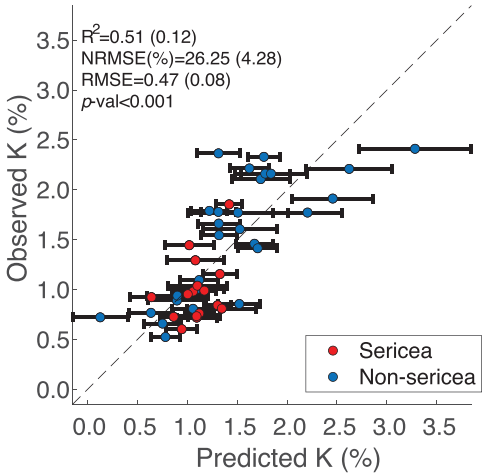

(h)

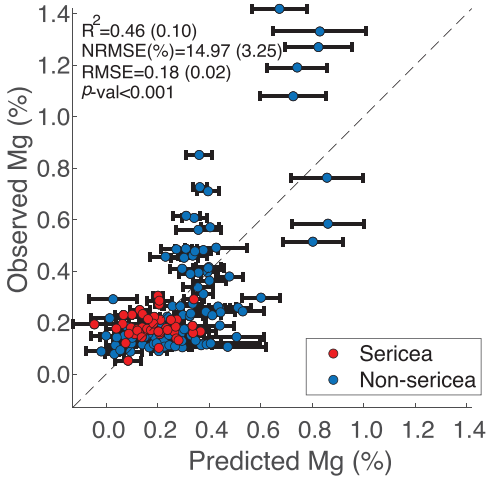

(i)

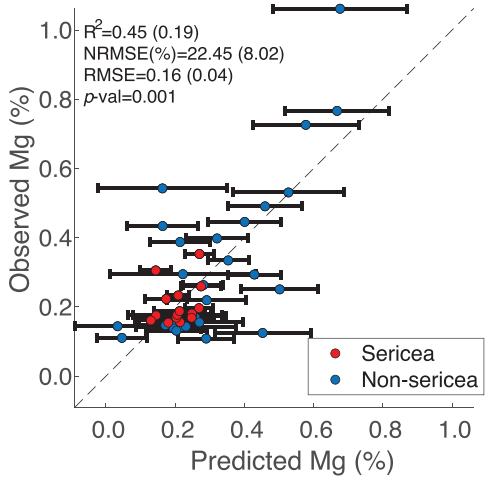

(j)

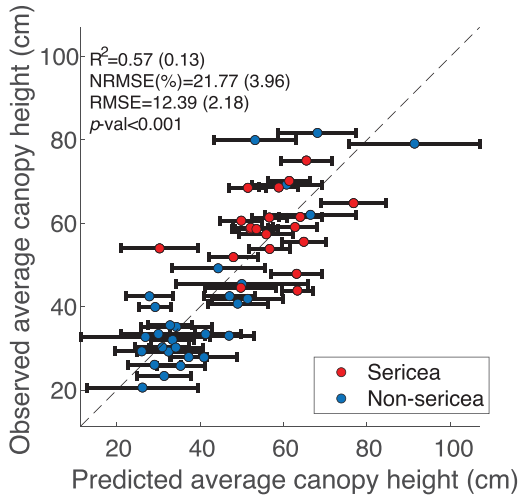

(k)

Fig. 6. (*continued*).

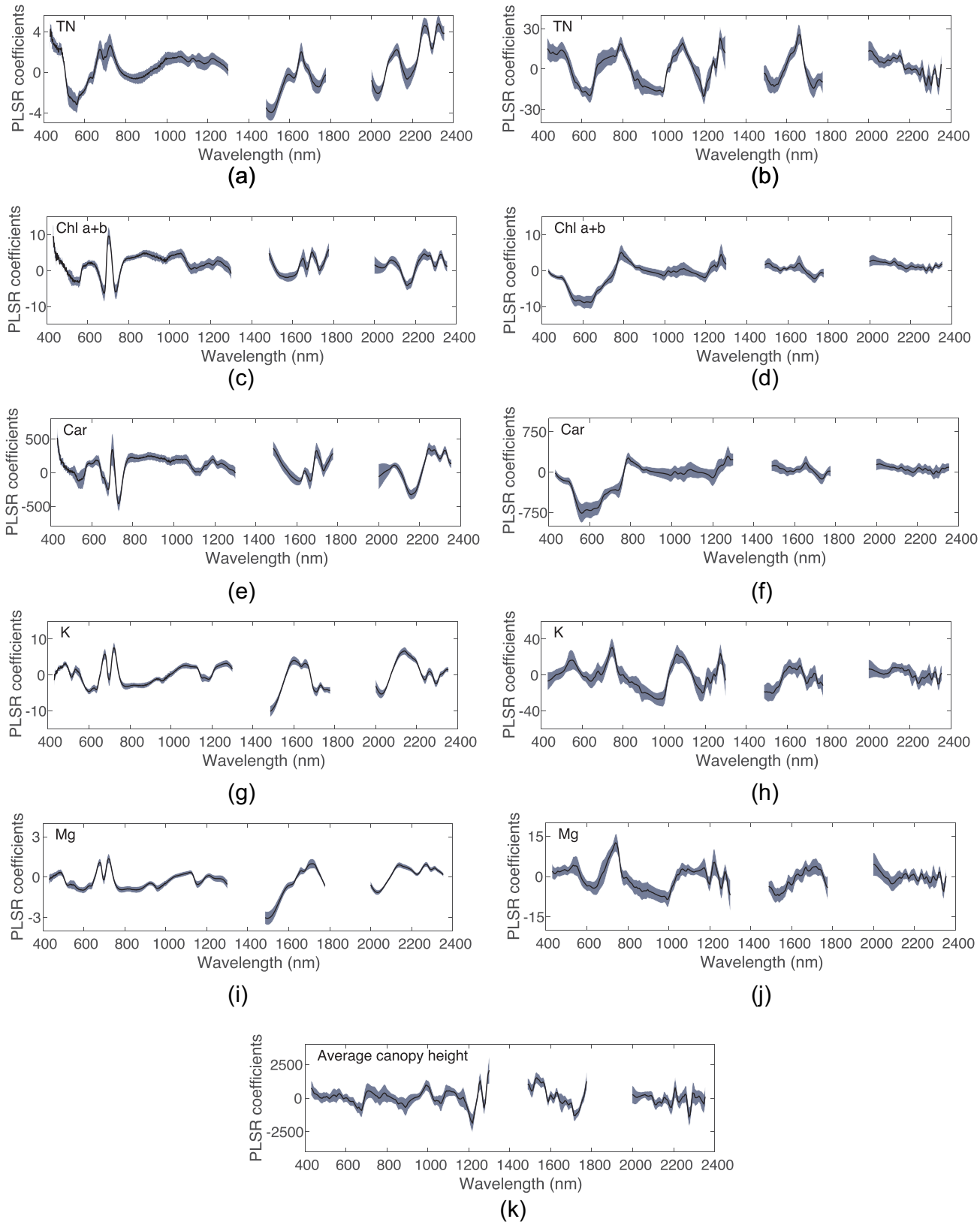

Fig. 7. PLSR coefficients obtained from leaf-level (left column) and canopy-level (right column) data. (a, c, e, g, i) For leaf-level data, independent variables are vector-normalized ASD reflectance data and dependent variables are leaf-level traits. (b, d, f, h, j) For canopy-level data, independent variables are vector-normalized airborne reflectance data and dependent variables are scaled-up patch-level traits. (k) For canopy height, only patch-level results obtained from airborne data are shown. Shaded regions show ±1 standard deviation from 300 permutations. Missing wavelength regions are water vapor absorption bands in the airborne data. For comparison purposes, water vapor absorption bands were excluded from leaf-level ASD data, although these data were not affected by atmospheric effects (because a contact leaf probe and an internal light source was used for leaf-level data collection). Functional trait acronyms: TN: total nitrogen, Chl a + b: Chlorophyll a + b, Car: total carotenoids, K: potassium, and Mg: magnesium.

Table 1
Performance of PLS-LDA classification using important functional traits based on the independent homogenous validation data set consisting of 78 patches, including 36 sericea patches and 42 non-sericea patches. In the PLS-LDA classification, each patch was considered as one data point. Numbers in the confusion matrix below represent the PLS-LDA model with median overall accuracy on 300 trials. Accuracy metrics are the average of 300 trials and numbers inside parentheses indicate ±1 standard deviation from 300 trials.

		Map			Producer's accuracy
		Sericea	Non-sericea	Total	
Field	Sericea	33	3	36	91.5% (±4.8%)
	Non-sericea	2	40	42	96.2% (±2.2%)
	Total	35	43	78	
User's accuracy		95.5% (±2.4%)	93.1% (±3.5%)		
Overall accuracy		94.0% (±2.0%)			
Kappa		0.87 (±0.04)			

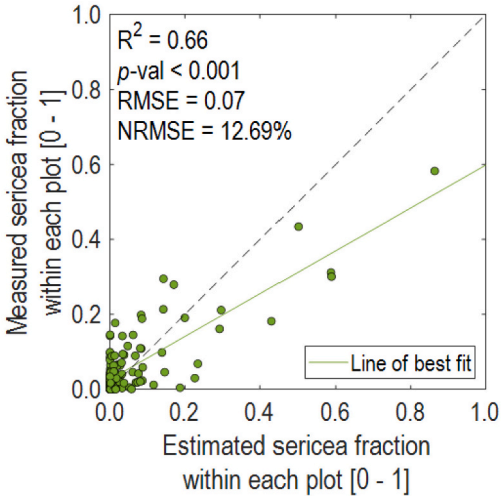

Fig. 8. Performance of PLS-LDA classification based on the heterogeneous validation data set consisting of 133 plots (see Section 2.2.2 for details). In this figure, 0 refers to 0% sericea cover within each plot and 1 refers to 100% sericea cover. Estimated sericea abundance fraction was calculated as the total number of pixels classified as sericea in all of 300 PLS-LDA models divided by the total number of pixels within each plot. The green line is the line of best fit and the dashed line is the 1:1 line. (For interpretation of the references to colour in this figure legend, the reader is referred to the web version of this article.)

range (~400–700 nm) and red edge region (~700–740 nm), although several bands within the near-infrared (~740–1100 nm) and shortwave infrared regions (~1100–2450 nm) were also selected. Specifically, out of 66 selected bands, 39 bands were within the visible range, which is about 97% of the total number of bands within this range in our airborne data set; five bands fell within the red edge region (83% of the total number of bands within the red edge region in our airborne data set). Additionally, 11 bands were near-infrared (20% of the total number of near-infrared bands in our airborne data set) and 11 bands were shortwave infrared (8% of the total number of bands in this region in our airborne data set). It is worth noting the significant contribution of bands in the photosynthetically active radiation (PAR) and red edge regions of airborne data at detecting sericea.

4. Discussion

Given the negative ecological and economic impacts of sericea, an operational IAS monitoring system is necessary for understanding invasion across large geographical extents. In this paper, by detecting grassland regions that have been invaded by sericea, we showed that there is a potential for developing such a monitoring system. Specifically, we first identified key functional traits that differentiated sericea from co-occurring native plants. These functional traits were then estimated throughout the study area using a PLSR approach applied to fine-resolution airborne hyperspectral data. Tested with field validation data, we found that remote estimation of these functional traits can successfully map sericea invasion in grasslands when used in a PLS-LDA classification approach.

4.1. Remote sensing can identify specific vegetation functional traits that contribute to the success of IAS

This research not only adapted the use of new methodologies for IAS detection but facilitated a deeper understanding of functional traits that aid mechanisms related to competition and tolerance strategies, specifically as IAS outcompete native species and succeed in a new community. Our results identified Car, Chl a + b, TN, and canopy height as well as two macronutrients (K and Mg) as the most important factors that contribute to distinguishing sericea from other species (Fig. 5). Surprisingly, TPC was not an important functional trait for distinguishing sericea from co-occurring native species, even though this plant is known to have high levels of a phenolic compound called tannin that cause digestive problems in ruminants such as cattle (Donnelly, 1954; Mosjidis et al., 1990; Silanikove et al., 2001).

Sericea had significantly higher photosynthetic and photoprotective pigments (Chl a + b and Car) compared to co-occurring native species (Fig. 4 and 6c-f), suggesting superior photophysiological performance of sericea compared to native plants. Specifically, Chl a + b can be viewed as a proxy for photosynthetic activity and Car, in addition to enhancing light harvesting for photosynthesis, has photoprotective properties and dissipates excess energy not used by the plant (Thayer and Björkman, 1990). As sericea forms canopy-dominant patches in full sun, enhanced photoprotection from Car likely aids in the species' invasive potential. Additionally, sericea had higher Chl a + b/Car ratio than co-occurring native species (Fig. S5 in Supplementary material). A large body of literature has indicated that a higher Chl a + b/Car ratio is linked to increased light use efficiency and photosynthetic activity (Gamon et al., 2016; Sims and Gamon, 2002) presumably because Car levels increase when plants are subjected to stress (Penuelas et al., 1995). Therefore, this finding suggests an adaptive response of sericea to the tallgrass ecosystem during environmental stress.

TN was significantly higher in sericea (Fig. 4 and 6a-b). In addition, TN was selected as one of the key traits for distinguishing sericea from co-occurring native plants (Fig. 5). Invasive legumes, including sericea, have a competitive advantage over native species, especially in nitrogen-poor soils, because of their nitrogen-fixing capabilities (Adams et al., 2016; Ritchie and Tilman, 1995). Therefore, selection of TN as a key trait appears very reasonable in the context of IAS tolerance and success strategies.

Additionally, sericea had higher canopy height compared to other species in our results (Fig. 4; Fig. 6k), and this trait was one of the important factors separating sericea from native plants (Fig. 5). Previous research has highlighted the role of canopy height on the success of sericea (Brandon et al., 2004). Specifically, sericea can form tall and

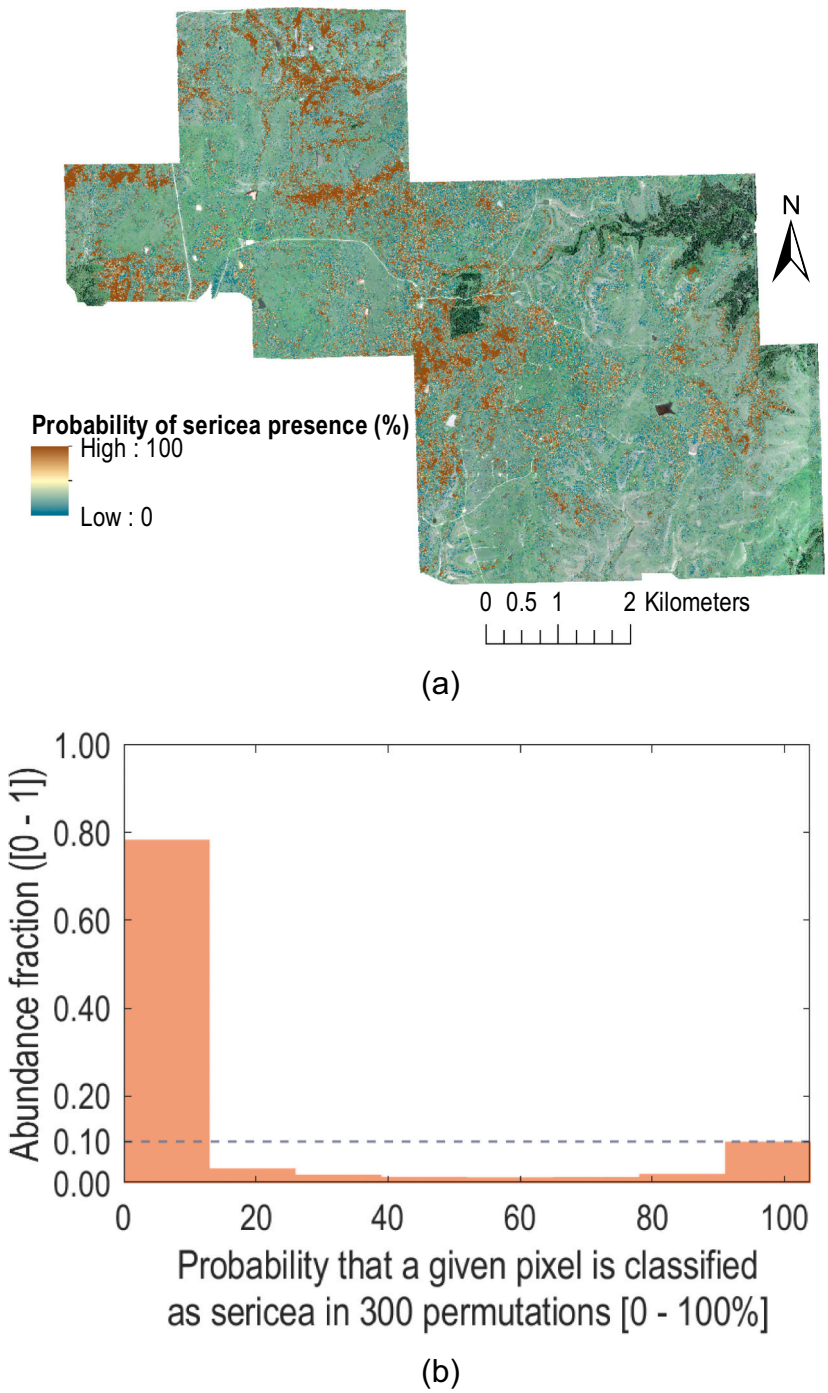

Fig. 9. (a) Sericea presence estimated based on 300 PLS-LDA classification models. Dark brown regions show pixels that were classified as sericea in all 300 model runs. Probability values are based on frequencies derived from 300 PLS-LDA models. The map is overlaid on an RGB composite of the study area. (b) Abundance fraction of sericea vs. non-sericea species (shown on y-axis; reported between 0 and 1). This histogram shows that approximately 10% of the study area is likely covered with sericea. Oak woodland land-cover (dark green vegetation cover in Fig. 9a) was not included in the calculations. (For interpretation of the references to colour in this figure legend, the reader is referred to the web version of this article.)

dense stands and therefore shade out other species. A remote sensing study in a small pasture, with total area of 0.6 km^2, at Cedar Creek Ranger District, Missouri used the maximal first-order spectral derivative in the 650–800 nm range to separate sericea from *Festuca arundinacea* (tall fescue; the dominant native species in the study area; Wang et al., 2008). Although the approach used in Wang et al. (2008) was fully empirical—meaning that underlying functional traits that distinguish sericea from tall fescue were not identified—separability of sericea from tall fescue was attributed to sericea's higher canopy height, density, and chlorophyll content. Our results confirmed the hypothesis set forth by Wang et al. (2008) and successfully identified canopy height and Chl a + b as important vegetation functional traits to map sericea invasion. Overall, our experiment demonstrated that there is promising potential for imaging spectroscopy to identify vegetation functional traits that lead to the success of IAS.

The central hypothesis of this experiment was that vegetation functional traits, including biochemical, physiological, and structural traits affect spectral signatures (Ustin and Gamon, 2010). However, phenology—temporal variation in biochemical, physiological, and structural traits—was not documented in our experiment, solely because the significant cost of multi-temporal airborne and field data collection campaigns precluded us from repeating these measurements over time. Previous studies have provided critical evidence that remote sensing signals vary significantly as a result of phenology (Bradley, 2014; Pettorelli et al., 2005; Wang et al., 2005). Similarly, in-situ measurement of a few vegetation attributes (gas exchange, chlorophyll fluorescence,

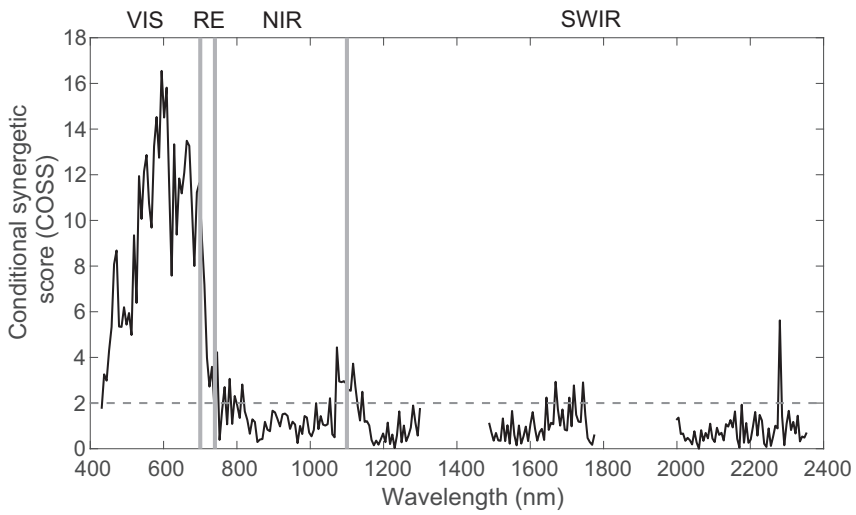

Fig. 10. COSS scores showing the importance of each spectral band in airborne data at separating sericea patches from non-sericea patches. Dashed line shows cutoff COSS value of 2. Vertical grey lines show wavelengths at 700 nm, 740 nm, and 1100 nm. Spectral region acronyms: VIS: visible, RE: red edge, NIR: near-infrared, and SWIR: shortwave infrared. (For interpretation of the references to colour in this figure legend, the reader is referred to the web version of this article.)

plant water status, and specific leaf area) has shown significant temporal variations in the functional traits of sericea and dominant species at TGPP (Allred et al., 2010), which can potentially affect distinguishing sericea from other native species using remotely sensed data. These results, collectively, support the need for developing multi-temporal experiments to test the generalizability of our IAS detection approach over time, especially in the face of rapid global change.

4.2. Remote detection of sericea: From key traits to key spectral bands

Our results indicated the importance of almost all the visible and red edge bands as well as portions of near-infrared and shortwave infrared regions at distinguishing sericea from non-sericea species in our airborne data (Fig. 10). Considering the list of key traits that were deemed important for separating sericea from non-sericea species (Fig. 5), we expected the selection of these bands, particularly those within the PAR and red edge regions.

Specifically, Chl a + b and Car—two traits with the highest COSS scores—have well-defined absorption features within the PAR region. Chlorophyll a has strong absorption features near 430 nm and 660–680 nm, chlorophyll *b* exhibits absorption features near 450 and 640 nm, and Car strongly absorbs radiation in wavelengths shorter than 550 nm (Blackburn, 2002; Curran, 1989; Fourty et al., 1996; Kokaly et al., 2009; Ustin et al., 2009). Confirming the findings of previous studies, our leaf-level PLSR analysis exhibited some of these absorption features, including the absorption feature near 680 nm (Fig. 7c; Fig. S6C in Supplementary material). In our patch-level PLSR analysis (i.e., airborne imagery), the majority of important wavelengths for estimating Chl a + b and Car were those within the PAR region (Fig. 7d and f; Fig. S6D and F in Supplementary material), which further fortifies our assumption that the separability of sericea from non-sericea species was partly due to differences in photosynthetic pigment content. In addition to Chl a + b and Car, TN—the other important trait at separating sericea from non-sericea species—may have contributed to the selection of bands within the PAR region through nitrogen-containing photosynthetic pigments, such as chlorophyll (Curran, 1989; Wang et al., 2019).

Selection of bands within the red edge region in our airborne hyperspectral data (Fig. 10) can be attributed in part to Chl a + b and Car content. Exhibited features within the red edge region in our leaf- and canopy-level Chl a + b and Car PLSR models (Fig. 7c, e, and f; Fig. S6C-F in Supplementary material) matched findings of previous studies; of note is the feature near 740 nm which has been reported to be an important spectral region for estimating mass-based Chl a + b and Car (Wang et al., 2020).

We should note that linking selected spectral bands (Fig. 10) to important functional traits that separated sericea from non-sericea species (Fig. 5) is not always straightforward. Some functional traits do not have specific absorption features or their absorption features might overlap with those of other traits (Kokaly et al., 2009). For example, K—which was identified as an important trait in our analysis—can be estimated due to its association with TN and LMA (Reich et al., 1997; Wang et al., 2020; Wright et al., 2004). In addition, at canopy-level (i.e., airborne imagery), our ability to identify specific absorption features and retrieve functional traits can be affected by canopy structure, as reflectance retrieved from airborne imagery is influenced by canopy structural characteristics, such as leaf shape and orientation (Jacquemoud et al., 2009; Knyazikhin et al., 2013; Sullivan et al., 2013).

Overall, except for photosynthetic pigments, establishing direct links between selected spectral bands in our airborne hyperspectral data (Fig. 10) and key vegetation functional traits that separated sericea from non-sericea species (Fig. 5) was not straightforward. However, both the direct impacts of key vegetation functional traits on remotely sensed spectra (e.g., through absorption features of photosynthetic pigments) and their indirect impacts (through canopy structural effects or associations among traits) translated into spectral separability between sericea and non-sericea species in the PAR and red edge regions of remotely sensed data. This spectral separability, in turn, suggests that there might be promising opportunities for developing multi-band empirical approaches, similar to vegetation indices, to separate sericea from non-sericea species.

4.3. Proposed approach overestimated sericea cover in species-rich communities

Our classification approach detected homogeneous patches of sericea with very high accuracy (overall accuracy of 94% from our homogenous validation data set; Table 1). However, it overestimated sericea abundance fraction in our heterogeneous validation data set that was collected from species-rich plant communities (Fig. 8). Previous studies on remote detection of IAS have reported similar issues with over- or underestimation of target species (Lass et al., 2002; Lawrence et al., 2006). We posit that this uncertainty is partly due to two closely-related issues: mixed pixels and scale mismatch between grassland plant size and scale of remote sensing observations.

4.3.1. Issues of mixed pixels and scale mismatch between grassland plant size and spatial resolution of remote sensing observations

Unlike our first validation data set which included homogeneous plant communities, in our heterogeneous validation data set, sericea abundance fractions were measured in species-rich and heterogeneous plots and in most cases, sericea percent cover within a community was less than 10%. This indicates that the probability of having pure sericea pixels within these species-rich plots was low and the majority of pixels were mixed, meaning that a given pixel was presumably covered with more than one species. The issue of mixed pixels is even more limiting for grassland species as these plants are often smaller than the scale of remote sensing observations. For example, if the size of an individual sericea plant is approximately 15 cm by 15 cm (when viewed from above), it occupies approximately $1/40^{th}$ of a pixel in our airborne imagery.

Both of these issues are major challenges in remote detection of IAS in grasslands, especially for early eradication efforts when invasive plants are more likely to occur in low abundance mixed with native species. Although we strived to make the best of assets at our disposal to collect remotely sensed data with fine spatial resolution, the issues of mixed pixels and scale mismatch were still significant sources of uncertainty in our study. These issues are even more limiting for direct detection of IAS using current and forthcoming spaceborne imaging spectrometers, primarily due to their coarse spatial resolution (approximately 30 m). The challenges associated with scale mismatch between plant size and spatial resolution of remotely sensed data demonstrate the essential role of fine-resolution airborne hyperspectral data for direct mapping of IAS in grasslands and ecosystems with small-statured plants.

4.3.2. Recommendations to mitigate the impact of scale mismatch

We put forth two suggestions for mitigating the uncertainty associated with IAS cover estimation. First, assessing the effectiveness of spectral unmixing approaches (also known as subpixel classification) remains a potentially promising direction for improving direct detection of IAS (see Fig. S7 in Supplementary material). Subpixel methods not only have the potential to improve IAS abundance estimation but they may also improve the detection of small and sparse IAS patches which may be vital to the success of early eradication efforts (Moody and Mack, 1988). Second, in addition to feature fusion—for example, through PLSR which was tested in our study—decision fusion can also potentially improve IAS classification accuracy (Kuncheva et al., 2001; Mangai et al., 2010). While a single classifier may not perform well for specific data inputs, outcome of multiple classifiers are combined in a decision fusion approach instead of relying on one classifier. Therefore, we recommend using multiple classifiers and combining their outcome as a potential solution to achieve more accurate and unbiased IAS detection.

4.4. Implications for sericea management practices

Landowners strive to manage and slow down sericea spread. Management practices to control the spread of sericea have typically focused on using herbicides or mowing (Altom et al., 1992; Brandon et al., 2004; Koger et al., 2002; Stevens, 2002). These herbicides are often effective for only short periods of time (e.g., season-long) and do not eradicate sericea permanently (Sherrill, 2019), presumably due to sericea's high seed production. In addition, repeat applications of herbicide for sericea control might have negative impacts on native species and are costly. Mowing has also been suggested by land managers to slow the spread of sericea; however, previous work has suggested that mowing may actually benefit sericea (Brandon et al., 2004). As a result, landowners resort to traditional grassland management practices, including prescribed fire, to control the spread of sericea. But these management practices have been originally developed to address other goals, mainly maintaining dominant forage species for livestock production and have not shown success in controlling the spread of sericea (Sherrill, 2019). As such, alternative management practices based on synergistic application of prescribed fire and grazing (Fuhlendorf et al., 2012) have been recommended to control and eradicate sericea. Initial results have reported that these alternative approaches outperform traditional practices that are based on the application of herbicide or prescribed fire (Cummings et al., 2007; Sherrill, 2019). However, such alternative practices have mainly been applied and tested in relatively small regions. Therefore, effectiveness of different management practices at controlling the spread of sericea should be further tested over large areas.

Remote sensing can play a central role in this regard through mapping sericea invasion over large areas and identifying the underlying functional traits that contribute to the success of invasion. Our experiment can potentially have important implications for developing science-driven management efforts to suppress the spread of sericea and other IAS in grasslands. Eventually, this experiment, and other similar experiments, will provide deeper understanding of invasion patterns of IAS, including sericea, with significant societal and economic benefits, especially for farmers, ranchers, and conservationists.

5. Conclusions

In this paper, we examined the capability of hyperspectral remote sensing to map an invasive alien species, called sericea, in a natural grassland. Our COSS analysis indicated that Car, Chl a + b, TN, canopy height, K, and Mg contributed to the separation of sericea from co-occurring native species. These functional traits were then used in a PLS-LDA classification to detect sericea. Overall accuracy of the PLS-LDA approach at detecting homogeneous patches of sericea was 94% and sericea omission and commission errors both were low and approximately 9% and 5%, respectively. Our approach, however, overestimated sericea abundance fraction in species-rich plant communities. We presume this overestimation was partly due to mixed pixels and mismatch between plant size and spatial resolution of our remotely sensed data.

This experiment showed the potential of remote sensing methods to quantify vegetation functional traits associated with IAS success strategies. Among the functional traits that were considered important in distinguishing sericea from other co-occurring native species, sericea had significantly higher Car, Chl a + b, TN, and canopy height than native plants. Selection of these four functional traits was reasonable in the context of IAS tolerance and competitive strategies. Specifically, sericea had significantly higher photosynthetic pigment content (Chl a + b and Car) compared to native species, suggesting its superior photophysiological performance at TGPP. In addition, sericea is a nitrogen-fixing legume which gives it an advantage over other species, especially in nitrogen-poor soils. This invasive species is also taller than the majority of co-occurring native species at TGPP which reduces the amount of light captured by native species and therefore suppresses them.

The methodology and findings of this study can have important implications for IAS management practices. This is particularly important for private landowners affected by IAS, especially when their resources are already stretched thin. An IAS mapping effort is often followed by appropriate management practices to control or slow down encroachment. Performance of different commonly-used management practices at controlling the spread of IAS is not the same. Although some of these management regimes, such as those based on synergistic application of prescribed fire and grazing have shown promise in controlling IAS spread, they have mainly been tested and applied over relatively small regions. Therefore, remote sensing can be considered as a viable tool for testing the performance of different management practices on controlling the spread of IAS over large areas.

Author contributions

H.G., H.A., A.T., S.F., O.J., and R.H. designed and conceived the study. H.G., N.M., W.H., M.F., A.S., K.H., M.C., and D.G. contributed to fieldwork. N.M. and A.S. collected sericea abundance data. M.F. and A.

T. developed protocols for biochemical trait analysis. M.F., W.H., and M. C. processed leaf samples to quantify vegetation functional traits. H.G. analyzed the data. All authors contributed to writing the manuscript.

Declaration of Competing Interest

The authors declare that they have no known competing financial interests or personal relationships that could have appeared to influence the work reported in this paper.

Acknowlegements

Three anonymous reviewers provided invaluable recommendations that significantly improved the quality of our manuscript, and we sincerely thank them for their insightful comments. We express our sincere gratitude to The Nature Conservancy for facilitating this study. We thank Amanda Bressoud, Cooper Sherrill, Aaron Cumashot, Graham Bell, Richard Northey, Tony Brown, Laura Goodman, and Michael Palmer for assisting us during the early stages of this experiment. The authors also thank Jesse Schafer, Head of Operations of High Performance Computing Center at Oklahoma State University. Hamed Gholizadeh was supported by a NASA NIP award [80NSSC21K0941] and Oklahoma Center for the Advancement of Science and Technology (OCAST) Basic Plant Science Research program [PS20–004]. Samuel Fuhlendorf was supported by a United States Department of Agriculture (USDA) NIFA award [2019–68012-29819] and Groendyke Endowment. Amy Trowbridge was supported by a National Science Foundation (NSF) Division of Biological Infrastructure award [DBI 2021898]. William Hammond was supported by NSF GRFP program [1–653428]. Henry Adams was supported by McIntire Stennis USDA NIFA program [WNP00009]. Mention of trade names does not imply endorsement by the authors.

Appendix A. Supplementary data

Supplementary data to this article can be found online at https://doi.org/10.1016/j.rse.2022.112887.

References

Adams, M.A., Turnbull, T.L., Sprent, J.I., Buchmann, N., 2016. Legumes are different: leaf nitrogen, photosynthesis, and water use efficiency. Proc. Natl. Acad. Sci. 113, 4098–4103.
Ainsworth, E.A., Gillespie, K.M., 2007. Estimation of total phenolic content and other oxidation substrates in plant tissues using Folin–Ciocalteu reagent. Nat. Protoc. 2, 875–877.
Allred, B.W., Fuhlendorf, S.D., Monaco, T.A., Will, R.E., 2010. Morphological and physiological traits in the success of the invasive plant Lespedeza cuneata. Biol. Invasions 12, 739–749.
Altom, J.V., Stritzke, J.F., Weeks, D.L., 1992. Sericea lespedeza (Lespedeza cuneata) control with selected postemergence herbicides. Weed Technol. 6, 573–576.
Andrew, M.E., Ustin, S.L., 2008. The role of environmental context in mapping invasive plants with hyperspectral image data. Remote Sens. Environ. 112, 4301–4317.
Asner, G.P., Martin, R.E., 2009. Spectral and chemical analysis of tropical forests: scaling from leaf to canopy levels. Remote Sens. Environ. 112, 3958–3970.
Ball, D.M., Hoveland, C.S., Lacefield, G.D., 2002. Southern Forages: Modern Concepts for Forage Crop Management. Potash & Phosphate Institute and the Foundation for Agronomic Research, Norcross, GA, USA.
Barker, M., Rayens, W., 2003. Partial least squares for discrimination. J. Chem. 17, 166–173.
Berk, A., Anderson, G.P., Acharya, P.K., Bernstein, L.S., Muratov, L., Lee, J., Fox, M., Adler-Golden, S.M., Chetwynd Jr., J.H., Hoke, M.L., Lockwood, R.B., Gardner, J.A., Cooley, T.W., Borel, C.C., Lewis, P.E., Shettle, E.P., 2006. MODTRAN5: 2006 update. In: Algorithms and Technologies for Multispectral, Hyperspectral, and Ultraspectral Imagery XII, Defense and Security Symposium. International Society for Optics and Photonics, Orlando, FL, USA, p. 62331F.
Blackburn, G.A., 2002. Remote sensing of forest pigments using airborne imaging spectrometer and LIDAR imagery. Remote Sens. Environ. 82, 311–321.
Bolch, E.A., Santos, M.J., Ade, C., Khanna, S., Basinger, N.T., Reader, M.O., Hestir, E.L., 2020. Remote detection of invasive alien species. In: Cavender-Bares, J., Gamon, J. A., Townsend, P.A. (Eds.), Remote Sensing of Plant Biodiversity. Springer Nature, Springer, New York, pp. 267–307.
Bradley, B.A., 2014. Remote detection of invasive plants: a review of spectral, textural and phenological approaches. Biol. Invasions 16, 1411–1425.
Bradley, B.A., Blumenthal, D.M., Wilcove, D.S., Ziska, L.H., 2010. Predicting plant invasions in an era of global change. Trends Ecol. Evol. 25, 310–318.
Bradley, B.A., Curtis, C.A., Fusco, E.J., Abatzoglou, J.T., Balch, J.K., Dadashi, S., Tuanmu, M.-N., 2018. Cheatgrass (*Bromus tectorum*) distribution in the intermountain Western United States and its relationship to fire frequency, seasonality, and ignitions. Biol. Invasions 20, 1493–1506.
Brandon, A.L., Gibson, D.J., Middleton, B.A., 2004. Mechanisms for dominance in an early successional old field by the invasive non-native Lespedeza cuneata (Dum. Cours.) G. Don. Biol. Invasions 6, 483–493.
Brereton, R.G., 2009. Chemometrics for Pattern Recognition. John Wiley & Sons.
Cline, G.R., Silvernail, A.F., 1997. Effects of soil acidity on the growth of sericea lespedeza. J. Plant Nutr. 20, 1657–1666.
Cohen, J., 1960. A coefficient of agreement for nominal scales. Educ. Psychol. Meas. 20, 37–46.
Coppedge, B., Engle, D., Toepfer, C., Shaw, J., 1998. Effects of seasonal fire, bison grazing and climatic variation on tallgrass prairie vegetation. Plant Ecol. 139, 235–246.
Cummings, D.C., Fuhlendorf, S.D., Engle, D.M., 2007. Is altering grazing selectivity of invasive forage species with patch burning more effective than herbicide treatments? Rangel. Ecol. Manag. 60, 253–260.
Curran, P.J., 1989. Remote sensing of foliar chemistry. Remote Sens. Environ. 30, 271–278.
De Las Rivas, J., Abadía, A., Abadia, J., 1989. A new reversed phase-HPLC method resolving all major higher plant photosynthetic pigments. Plant Physiol. 91, 190–192.
Diagne, C., Leroy, B., Vaissière, A.-C., Gozlan, R.E., Roiz, D., Jarić, I., Salles, J.-M., Bradshaw, C.J., Courchamp, F., 2021. High and rising economic costs of biological invasions worldwide. Nature 592, 571–576.
Donnelly, E.D., 1954. Some factors that affect palatability in sericea lespedeza Lespedeza cuneata. Agron. J. 46, 96–97.
Dukes, J.S., Mooney, H.A., 1999. Does global change increase the success of biological invaders? Trends Ecol. Evol. 14, 135–139.
Eschtruth, A.K., Battles, J.J., 2009. Assessing the relative importance of disturbance, herbivory, diversity, and propagule pressure in exotic plant invasion. Ecol. Monogr. 79, 265–280.
Everitt, J.H., Pettit, R.D., Alaniz, M.A., 1987. Remote sensing of broom snakeweed (Gutierrezia sarothrae) and spiny aster (Aster spinosus). Weed Sci. 295–302.
Feilhauer, H., Asner, G.P., Martin, R.E., Schmidtlein, S., 2010. Brightness-normalized partial least squares regression for hyperspectral data. J. Quant. Spectrosc. Radiat. Transf. 111, 1947–1957.
Fourty, T., Baret, F., Jacquemoud, S., Schmuck, G., Verdebout, J., 1996. Leaf optical properties with explicit description of its biochemical composition: direct and inverse problems. Remote Sens. Environ. 56, 104–117.
Fuhlendorf, S., Engle, D., 2004. Application of the fire–grazing interaction to restore a shifting mosaic on tallgrass prairie. J. Appl. Ecol. 41, 604–614.
Fuhlendorf, S.D., Engle, D.M., Kerby, J., Hamilton, R., 2009. Pyric herbivory: rewilding landscapes through the recoupling of fire and grazing. Conserv. Biol. 23, 588–598.
Fuhlendorf, S.D., Engle, D.M., Elmore, R.D., Limb, R.F., Bidwell, T.G., 2012. Conservation of pattern and process: developing an alternative paradigm of rangeland management. Rangel. Ecol. Manag. 65, 579–589.
Gamon, J.A., Huemmrich, K.F., Wong, C.Y., Ensminger, I., Garrity, S., Hollinger, D.Y., Noormets, A., Peñuelas, J., 2016. A remotely sensed pigment index reveals photosynthetic phenology in evergreen conifers. Proc. Natl. Acad. Sci. 113, 13087–13092.
Glenn, N.F., Mundt, J.T., Weber, K.T., Prather, T.S., Lass, L.W., Pettingill, J., 2005. Hyperspectral data processing for repeat detection of small infestations of leafy spurge. Remote Sens. Environ. 95, 399–412.
Hamilton, R.G., 2007. Restoring heterogeneity on the Tallgrass Prairie Preserve: Applying the fire-grazing interaction model. In: Masters, R.E., Galley, K.E.M. (Eds.), Proceedings of the 23rd Tall Timbers Fire Ecology Conference: Fire in Grassland and Shrubland Ecosystems. Tall Timbers Research Station Tallahassee, Tallahassee, FL, USA, pp. 163–169.
He, K.S., Bradley, B.A., Cord, A.F., Rocchini, D., Tuanmu, M.N., Schmidtlein, S., Turner, W., Wegmann, M., Pettorelli, N., 2015. Will remote sensing shape the next generation of species distribution models? Remote Sens. Ecol. Conserv. 1, 4–18.
Hoveland, C., Windham, W., Boggs, D., Durham, R., Calvert, G., Newsome, J., Dobson Jr., J., Owsley, M., 1990. Sericea lespedeza production in Georgia. Georg. Exp. Station Res. Bull. 393.
Huang, C.Y., Geiger, E.L., 2008. Climate anomalies provide opportunities for large-scale mapping of non-native plant abundance in desert grasslands. Divers. Distrib. 14, 875–884.
Hulme, P.E., 2009. Trade, transport and trouble: managing invasive species pathways in an era of globalization. J. Appl. Ecol. 46, 10–18.
Hunt Jr., E.R., McMurtrey III, J.E., Williams, A.E.P., Corp, L.A., 2004. Spectral characteristics of leafy spurge (Euphorbia esula) leaves and flower bracts. Weed Sci. 492–497.
Ishii, J., Washitani, I., 2013. Early detection of the invasive alien plant Solidago altissima in moist tall grassland using hyperspectral imagery. Int. J. Remote Sens. 34, 5926–5936.
Jacquemoud, S., Verhoef, W., Baret, F., Bacour, C., Zarco-Tejada, P.J., Asner, G.P., François, C., Ustin, S.L., 2009. PROSPECT+SAIL models: a review of use for vegetation characterization. Remote Sens. Environ. 113, S56–S66.
Katabuchi, M., 2015. LeafArea: an R package for rapid digital image analysis of leaf area. Ecol. Res. 30, 1073–1077.
Kettenring, K.M., Adams, C.R., 2011. Lessons learned from invasive plant control experiments: a systematic review and meta-analysis. J. Appl. Ecol. 48, 970–979.

Knyazikhin, Y., Schull, M.A., Stenberg, P., Mõttus, M., Rautiainen, M., Yang, Y., Marshak, A., Carmona, P.L., Kaufmann, R.K., Lewis, P., 2013. Hyperspectral remote sensing of foliar nitrogen content. Proc. Natl. Acad. Sci. 110, E185–E192.
Koger, C.H., Stritzke, J.F., Cummings, D.C., 2002. Control of sericea lespedeza (Lespedeza cuneata) with triclopyr, fluroxypyr, and metsulfuron. Weed Technol. 16, 893–900.
Kokaly, R.F., Asner, G.P., Ollinger, S.V., Martin, M.E., Wessman, C.A., 2009. Characterizing canopy biochemistry from imaging spectroscopy and its application to ecosystem studies. Remote Sens. Environ. 113, S78–S91.
Kruskal, W.H., Wallis, W.A., 1952. Use of ranks in one-criterion variance analysis. J. Am. Stat. Assoc. 47, 583–621.
Kuncheva, L.I., Bezdek, J.C., Duin, R.P., 2001. Decision templates for multiple classifier fusion: an experimental comparison. Pattern Recogn. 34, 299–314.
Landis, J.R., Koch, G.G., 1977. The measurement of observer agreement for categorical data. Biometrics 159–174.
Lass, L.W., Thill, D.C., Shafii, B., Prather, T.S., 2002. Detecting spotted knapweed (Centaurea maculosa) with hyperspectral remote sensing technology1. Weed Technol. 16, 426–432.
Lawrence, R.L., Wood, S.D., Sheley, R.L., 2006. Mapping invasive plants using hyperspectral imagery and Breiman Cutler classifications (RandomForest). Remote Sens. Environ. 100, 356–362.
Li, H.-D., Zeng, M.-M., Tan, B.-B., Liang, Y.-Z., Xu, Q.-S., Cao, D.-S., 2010. Recipe for revealing informative metabolites based on model population analysis. Metabolomics 6, 353–361.
Limb, R.F., Hickman, K.R., Engle, D.M., Norland, J.E., Fuhlendorf, S.D., 2007. Digital photography: reduced investigator variation in visual obstruction measurements for southern tallgrass prairie. Rangel. Ecol. Manag. 60, 548–552.
Mack, R.N., Simberloff, D., Mark Lonsdale, W., Evans, H., Clout, M., Bazzaz, F.A., 2000. Biotic invasions: causes, epidemiology, global consequences, and control. Ecol. Appl. 10, 689–710.
Mäkinen, H., Kaseva, J., Virkajärvi, P., Kahiluoto, H., 2015. Managing resilience of forage crops to climate change through response diversity. Field Crop Res. 183, 23–30.
Mangai, U.G., Samanta, S., Das, S., Chowdhury, P.R., 2010. A survey of decision fusion and feature fusion strategies for pattern classification. IETE Tech. Rev. 27, 293–307.
Marquard, E., Weigelt, A., Temperton, V.M., Roscher, C., Schumacher, J., Buchmann, N., Fischer, M., Weisser, W.W., Schmid, B., 2009. Plant species richness and functional composition drive overyielding in a six-year grassland experiment. Ecology 90, 3290–3302.
MATLAB, 2020. version 9.9.0 (R2020b). The MathWorks Inc., Natick, Massachusetts, USA.
Mitchell, J.J., Glenn, N.F., 2009. Leafy spurge (Euphorbia esula) classification performance using hyperspectral and multispectral sensors. Rangel. Ecol. Manag. 62, 16–27.
Moody, M.E., Mack, R.N., 1988. Controlling the spread of plant invasions: the importance of nascent foci. J. Appl. Ecol. 1009–1021.
Mooney, H., Hobbs, R.J., 2000. Invasive Species in a Changing World. Island Press, Washington, D.C.
Mosjidis, C.O.H., Peterson, C., Mosjidis, J., 1990. Developmental differences in the location of polyphenols and condensed tannins in leaves and stems of sericea lespedeza, Lespedeza cuneata. Ann. Bot. 65, 355–360.
Pejchar, L., Mooney, H.A., 2009. Invasive species, ecosystem services and human well-being. Trends Ecol. Evol. 24, 497–504.
Penuelas, J., Baret, F., Filella, I., 1995. Semi-empirical indices to assess carotenoids/chlorophyll a ratio from leaf spectral reflectance. Photosynthetica 31, 221–230.
Pettorelli, N., Vik, J.O., Mysterud, A., Gaillard, J.-M., Tucker, C.J., Stenseth, N.C., 2005. Using the satellite-derived NDVI to assess ecological responses to environmental change. Trends Ecol. Evol. 20, 503–510.
Pieters, A.J., 1938. Legumes in soil conservation practices. In: USDA Leaflet, 163, p. 8.
Pieters, A.J., Henson, P., Adams, W.E., 1950. Lespedeza sericea and other perennial lespedezas for forage and soil conservation. In: USDA Circular 863. United States Department of Agriculture, Washington D.C., p. 48
Pimentel, D., McNair, S., Janecka, J., Wightman, J., Simmonds, C., O'connell, C., Wong, E., Russel, L., Zern, J., Aquino, T., 2001. Economic and environmental threats of alien plant, animal, and microbe invasions. Agric. Ecosyst. Environ. 84, 1–20.
Reich, P.B., Walters, M.B., Ellsworth, D.S., 1997. From tropics to tundra: global convergence in plant functioning. Proc. Natl. Acad. Sci. 94, 13730–13734.
Richter, R., Schläpfer, D., 2002. Geo-atmospheric processing of airborne imaging spectrometry data. Part 2: atmospheric/topographic correction. Int. J. Remote Sens. 23, 2631–2649.
Ritchie, M.E., Tilman, D., 1995. Responses of legumes to herbivores and nutrients during succession on a nitrogen-poor soil. Ecology 76, 2648–2655.
Rosenfield, G.H., Fitzpatrick-Lins, K., 1986. A coefficient of agreement as a measure of thematic classification accuracy. Photogramm. Eng. Remote. Sens. 52, 223–227.
Serbin, S.P., Townsend, P.A., 2020. Scaling functional traits from leaves to canopies. In: Cavender-Bares, J., Gamon, J.A., Townsend, P.A. (Eds.), Remote Sensing of Biodiversity. Springer Nature, Springer, New York, pp. 43–82.
Sherrill, C.W., 2019. Analyzing sericea lespedeza (lespedeza cuneata) management practices and the importance of forbs in the diet of cattle and bison on tallgrass prairie. In: Natural Resource Ecology and Management. Oklahoma State University, Stillwater, OK. Master's Thesis.
Silanikove, N., Perevolotsky, A., Provenza, F.D., 2001. Use of tannin-binding chemicals to assay for tannins and their negative postingestive effects in ruminants. Anim. Feed Sci. Technol. 91, 69–81.
Sims, D.A., Gamon, J.A., 2002. Relationships between leaf pigment content and spectral reflectance across a wide range of species, leaf structures and developmental stages. Remote Sens. Environ. 81, 337–354.
Singh, N., Glenn, N.F., 2009. Multitemporal spectral analysis for cheatgrass (Bromus tectorum) classification. Int. J. Remote Sens. 30, 3441–3462.
Singh, A., Serbin, S.P., McNeil, B.E., Kingdon, C.C., Townsend, P.A., 2015. Imaging spectroscopy algorithms for mapping canopy foliar chemical and morphological traits and their uncertainties. Ecol. Appl. 25, 2180–2197.
Stevens, S., 2002. Element stewardship abstract for Lespedeza cuneata (Dumont-Cours.) G. Don Sericea Lespedeza, Chinese Bush Cover. In: Tu, M., Rice, B., Randal, J. (Eds.), Arlington. The Nature Conservancy's Wildland Invasive Species Team, Department of Vegetable Crops and Weed Sciences, VA, USA.
Stitt, R.E., Clarke, I.D., 1941. The relation of tannin content of sericea lespedeza to season. J. Am. Soc. Agr. 739–742.
Sullivan, F.B., Ollinger, S.V., Martin, M.E., Ducey, M.J., Lepine, L.C., Wicklein, H.F., 2013. Foliar nitrogen in relation to plant traits and reflectance properties of New Hampshire forests. Can. J. For. Res. 43, 18–27.
Thayer, S.S., Björkman, O., 1990. Leaf xanthophyll content and composition in sun and shade determined by HPLC. Photosynth. Res. 23, 331–343.
Tilman, D., Knops, J., Wedin, D., Reich, P., Ritchie, M., Siemann, E., 1997. The influence of functional diversity and composition on ecosystem processes. Science 277, 1300–1302.
TNC, . Joseph H. Williams Tallgrass Prairie Preserve. In. https://www.nature.org/en-us/get-involved/how-to-help/places-we-protect/tallgrass-prairie-preserve/ (accessed on July 16, 2021). The Nature Conservancy.
Ustin, S.L., Gamon, J.A., 2010. Remote sensing of plant functional types. New Phytol. 186, 795–816.
Ustin, S.L., Gitelson, A.A., Jacquemoud, S., Schaepman, M., Asner, G.P., Gamon, J.A., Zarco-Tejada, P., 2009. Retrieval of foliar information about plant pigment systems from high resolution spectroscopy. Remote Sens. Environ. 113, S67–S77.
Wang, J., Rich, P.M., Price, K.P., Kettle, W.D., 2005. Relations between NDVI, grassland production, and crop yield in the central Great Plains. Geocart. Int. 20, 5–11.
Wang, C., Zhou, B., Palm, H.L., 2008. Detecting invasive sericea lespedeza (Lespedeza cuneata) in Mid-Missouri pastureland using hyperspectral imagery. Environ. Manag. 41, 853–862.
Wang, Z., Townsend, P.A., Schweiger, A.K., Couture, J.J., Singh, A., Hobbie, S.E., Cavender-Bares, J., 2019. Mapping foliar functional traits and their uncertainties across three years in a grassland experiment. Remote Sens. Environ. 221, 405–416.
Wang, Z., Chlus, A., Geygan, R., Ye, Z., Zheng, T., Singh, A., Couture, J.J., Cavender-Bares, J., Kruger, E.L., Townsend, P.A., 2020. Foliar functional traits from imaging spectroscopy across biomes in eastern North America. New Phytol. 228, 494–511.
Williamson, M., 1999. Invasions. Ecography 22, 5–12.
Wold, S., Sjöström, M., Eriksson, L., 2001. PLS-regression: a basic tool of chemometrics. Chemom. Intell. Lab. Syst. 58, 109–130.
Wright, I.J., Reich, P.B., Westoby, M., Ackerly, D.D., Baruch, Z., Bongers, F., Cavender-Bares, J., Chapin, T., Cornelissen, J.H., Diemer, M., 2004. The worldwide leaf economics spectrum. Nature 428, 821.
Yang, C., Everitt, J., 2010. Comparison of hyperspectral imagery with aerial photography and multispectral imagery for mapping broom snakeweed. Int. J. Remote Sens. 31, 5423–5438.